(Affymetrix), which was purified using RNeasy Mini Kit (QIAGEN). The labeled cRNA was hydrolyzed in fragmentation buffer (40 mM Tris-acetate pH8.1, 100 mM KOAc, 30 mM MgOAc) to a size of approximately 35–200 nucleotides.

Ten microgram of the fragmented cRNA was hybridized with the Murine Genome U74AV2 array (Affymetrix) in hybridization cocktail (0.05 ug/uL cRNA, 50 pM control oligonucleotide B2, 1.5 pM bioB, 5 pM bioC, 25 pM bioD, 100 pM cre, 0.1 mg/mL herring sperm DNA, 0.5 mg/mL acetylated BSA, 100 mM MES, 1 M Na+, 20 mM EDTA, 0.01% Tween20). Hybridization was carried out overnight (16 h) at 45 °C, followed by washing, and staining with streptavidin-phycoerythrin (SAPE, Molecular Proves, OR, USA). Hybridization assay procedures including preparation of solutions were carried out as described in the Affymetrix GeneChip Expression Analysis Technical Manual. The distribution of fluorescent material on the array was determined using a confocal laser scanner (GeneArray Scanner, Affymetrix).

Array data processing

Signal quantification, background adjustment, judgment of detection call and other analysis were performed using the Microarray Suite (MAS) ver. 5.0 (Affymetrix). All arrays were globally scaled to a target value of 200. Genes were only considered for further analysis, if their corresponding probe sets had a signal intensity over 300 and their detection call were P (present). Pair-wise comparison analysis was performed between SZ-treated hepatocytes and control hepatocytes. The signal log ratio (SLR) was calculated for each probe set using the following formula: $\log_2$ (signal intensity in SZ-treated mice/that in control mice). Probe sets with SLR greater or equal to 1.0 was judged as 'up-regulated'. On the other hand, probe sets with SLR less or equal to −1.0 was judged as 'down-regulated'.

Annotation information on the probe sets on the U74A V.2 array was downloaded from the NetAffyx provided by Affymetrix. The probe sets judged as 'up-regulated' or 'down-regulated' were categorized according to the annotation information and protein information from Protein Knowledgebase provided by Swiss Institute of Bioinformatics (Swiss-Prot).

Results

Cell survival

Fig. 1 shows the concentration–response curve of the cell survival analysis. IC50 value in 6 h exposure was 62 mM and that in 24 h exposure was 7 mM.

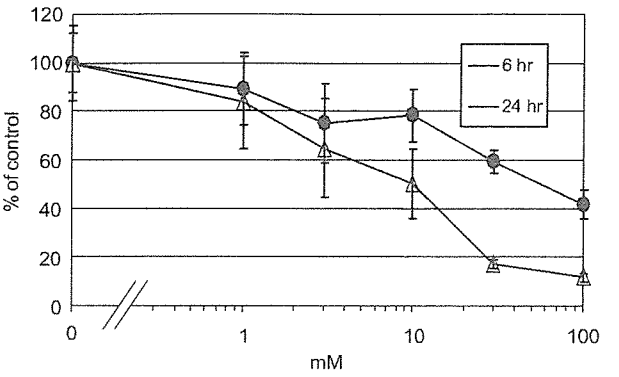

Fig. 1. Cell survival rate of mouse primary cultured hepatocytes exposed with SZ. Closed circle expressed the concentration–response curve of 6 h exposure, and open triangle expressed the one of 24 h exposure. The 50% inhibition concentration (IC50) values were approximately 62 and 7 mM at 6 h exposure and 24 h exposure, respectively.

Morphological examination

Apparent differences were not observed under the phase contrast microscope between the SZ-treated hepatocytes and the control hepatocytes. Only slight decrease in the cell density was observed in 100 mM-24 h exposure group.

Light microscopic analysis using semi-thin toluidin blue stained sections was performed on 1–10 mM exposure groups. Margination of nuclear chromatin was observed in the hepatocytes treated with SZ for 24 h at doses of 3 and 10 mM (Fig. 2). No other changes were observed.

Compaction and margination of nuclear chromatin in the SZ group were also observed under the electron microscope (Fig. 3). Some hepatocytes in the SZ group showed increases in lipid droplets, lysosome and peroxisome, and the structure of crista of some mitochondria were obscure, although most hepatocytes showed no apparent difference in the cytoplasm.

GeneChip analysis

Comparison analysis of the expression profiles was performed between SZ-treated hepatocytes and control hepatocytes. Time points and concentrations were 1 mM-6 h, 1 mM-24 h and 3 mM-24 h exposure. Table 1 shows the number of the up-regulated (SLR > = 1.0) or the down-regulated (SLR < = −1.0) probe sets. The number of up-regulated probe sets were 16, 18 and 210, respectively. The number of down-regulated probe sets were 30, 20 and 278, respectively. Probe sets, of which SLR was over 1.5 or was under −1.5, were picked up and tabulated in Table 2. The

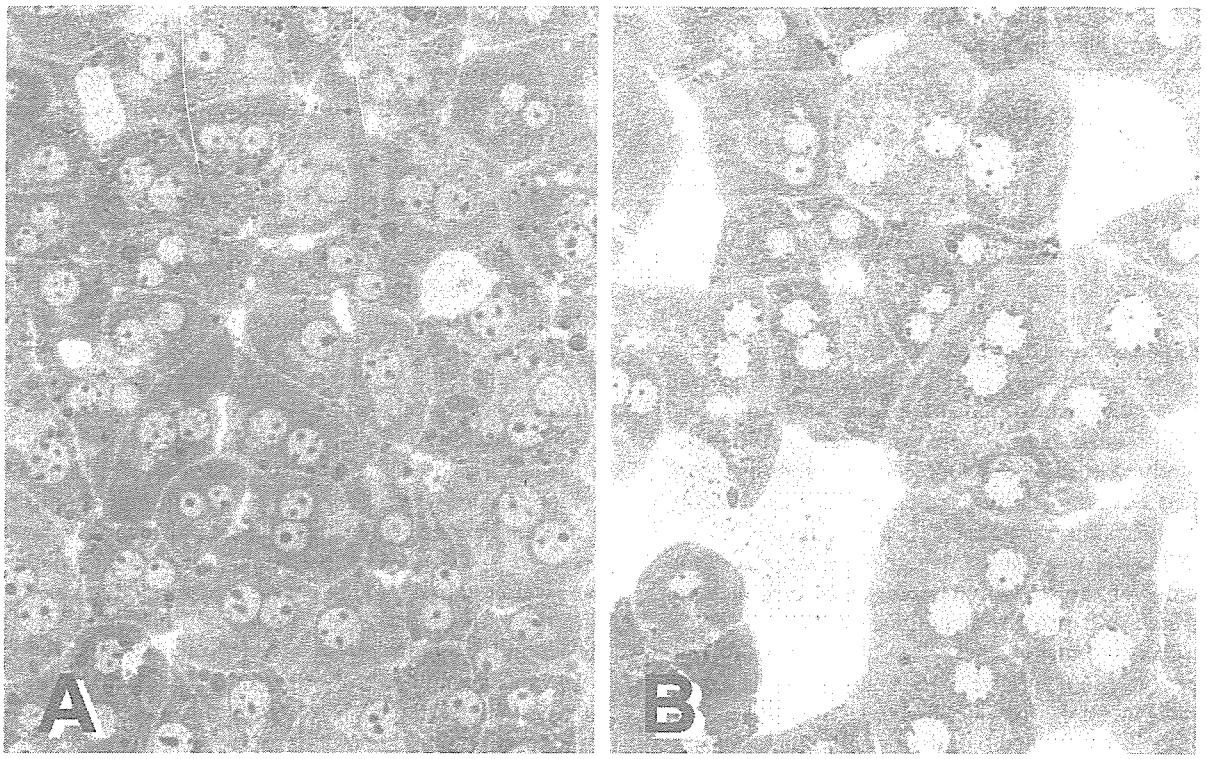

Fig. 2. Light microphotographs of primary cultured hepatocytes treated with vehicle (A) or 10 mM of SZ (B) for 24 h. Marked chromatin margination was observed in nuclei of the hepatocytes treated with SZ. Toluidin blue, × 500.

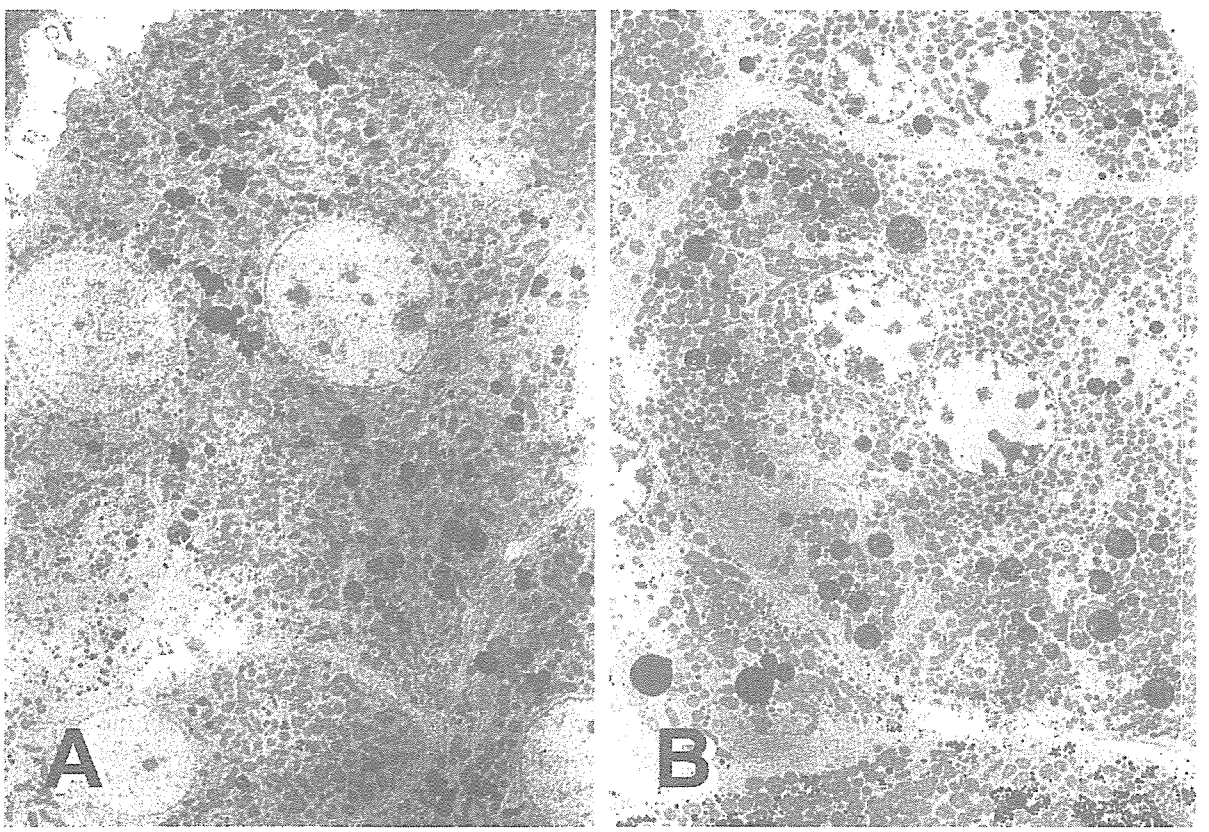

Fig. 3. Electron microphotographs of primary cultured hepatocytes treated with vehicle (A) or 10 mM of SZ (B) for 24 h. Compaction and margination of nuclear chromatin were observed in nuclei of the hepatocytes treated with SZ, × 1800.

Table 1. Number of up- or down-regulated genes in the primary cultured hepatocytes exposed to SZ

	1 mM 6 h	1 mM 24 h	3 mM 24 h
Up-regulated genes	16	18	210
Down-regulated genes	30	20	278

Up-regulated genes: signal $\log_2$ ratio to the control (SLR) > = 1.0. Down-regulated genes: signal $\log_2$ ratio to the control (SLR) < = −1.0.

regulated genes showed a broad range, but many of the up-regulated genes were categorized into cell cycle/apoptosis-related genes and stress response/xenobiotic metabolism-related genes. 'Growth arrest and DNA-damage-inducible 45' (GADD45), 'p53 apoptosis effector related to Pmp22' (perp), 'tumor necrosis factor receptor superfamily, member 6' (tnfrsf6) and 'RAD51-like 1' (Rad51l1) were of particular note. On the other hand, many of the down-regulated genes belonged to glucose, lipid and protein metabolism-related genes or immune/allergy related genes. '3-hydroxy-3-methylglutaryl-Coenzyme A synthase 1' (Hmgcs1), 'microsomal triglyceride transfer proteine' (Mttp), 'stearoyl-Coenzyme A desaturase 2' (Scd2) and other lipid metabolism-related genes were of particular note.

Discussion

Morphological examinations and gene expression analysis were performed on mouse primary hepatocytes exposed to SZ to clarify direct effects of the compound on hepatocytes.

IC50 value for cell survival at 6 and 24 h exposure were 62 and 7 mM, respectively, which were relatively higher values than other medical drugs, such as cisplatin, erythromycin, amiodarone, chlorpromazine, and so on, in similar evaluations using rat primary hepatocytes (Wang et al., 2002). We can say that SZ has weak direct cytotoxicity. SZ showed stronger cytotoxicity in tumor cell lines than in hepatocytes, approximately 1 mM in insulinoma cell line (Ledoux and Wilson, 1984), and around 0.4 mM in mouse lymphoma (Bhuyan, 1970).

Morphological examination revealed compaction and margination of nuclear chromatin, which were characteristics of early stage apoptosis. However, the apparent characteristics of apoptosis, i.e., nuclear fragmentation, cytoplasmic shrinkage or blebbing of the cell membrane, were not observed in this study. Those histopathological characteristics of apoptosis were not observed in SZ-treated mice (Kume et al., 2004). It is interesting that apoptosis-related genes were up-regulated both in vivo (Kume et al., in press) and in vitro, although the apparent apoptosis were not observed neither in vitro nor in vivo. Flament and Remacle (1987) reported ultrastructural changes observed in SZ-treated pancreatic islets in vitro. The changes were a slight increase in heterochromatin, swelling of nuclear membrane, dilatation of rough endoplasmic reticulum, and mitochondrial destruction, suggesting necrosis but not apoptosis. The mechanisms involved in islet cell damage and hepatocytes damage might be quite different.

Mitochondrial swelling is one of the characteristic morphological changes observed at 6 h after SZ treatment (Kume et al., 2004), which may be related to mitochondrial proliferation observed in the subacute or chronic phase (Kume et al., 1994a, b). In this study, mitochondria of some hepatocytes showed abnormal obscure crista, which might be related to mitochondrial damage, but no other mitochondrial changes were observed in vitro. Thus, we could not offer proof that the mitochondrial changes were a direct effect of SZ. However, there is some possibility that changes in mitochondrial morphology were difficult to detect in vitro in this study, because the mitochondrial shapes in vitro varied too much to differentiate a small change. Functional assays should be performed to clarify the direct effect of SZ on liver mitochondria.

Gene expression analysis revealed similar regulations of gene expression by SZ in in vivo (Kume et al., in press) and in vitro treatment, such as the up-regulation of cell cycle/apoptosis-related genes, the down-regulation of glucose, lipid and protein metabolism-related genes, and so on. Table 3 shows the in vivo and in vitro comparison, in which probe sets were picked up if their SLR were over 1.5 or were under −1.5 at representative time points (in vivo: 200 mg/kg 24 h after the administration, in vitro: 3 mM-24 h).

Among the up-regulated cell cycle/apoptosis-related genes, several major genes related to induction of cell cycle checkpoint and arrest were observed. These included growth arrest and DNA-damage-inducible 45 (GADD45), and cyclin-dependent kinase inhibitor 1A (Cdkn1a, p21). Cell cycle arrest was observed in vivo by immunohistochemical analysis, in which the ratio of the proliferating cell nuclear antigen (PCNA) positive hepatocytes was low at 24 and 48 h after the SZ-treatment (Kume et al., 2004). If we use a highly proliferative cell line rather than primary cultured hepatocytes, a decrease in cell proliferation may be observed in vitro as seen in other studies (Bhuyan, 1970; Capucci et al., 1995). Several genes related to induction of apoptosis were also up-regulated, which include 'Bcl2-associated X protein' (bax), 'apoptotic protease activating factor 1' (Apaf1), 'tumor necrosis factor receptor superfamily, member 6' (tnfrsf6), 'wild-type p53-induced gene 1' (wig1), 'transformed mouse 3T3 cell double minute 2' (mdm2) and 'p53 apoptosis effector

Table 2. Gene expression in primary cultured hepatocytes exposed with SZ

Title	GeneName	1 mM 6 h	1 mM 24 h	3 mM 24 h	Affy ID
Carbohydrate and lipid metabolism					
Cytosolic acyl-CoA thioesterase 1	Cte1	-0.2	0.9	-1.5	103581_at
Cytochrome P450, 51	Cyp51	-0.2	-0.9	-1.7	94916_at
Fatty acid binding protein 1, liver	Fabp1	0.4	0	-1.6	94075_at
Glucokinase	Gck	0	-0.8	-1.9	102651_at
3-hydroxy-3-methylglutaryl-Coenzyme A synthase 1	Hmgcs1	-0.6	-0.7	-1.5	94325_at
Isopentenyl-diphosphate delta isomerase	Idi1	0.1	-0.8	-1.5	96269_at
Microsomal triglyceride transfer protein	Mttp	-0.3	-0.1	-1.7	104448_at
NAD(P) dependent steroid dehydrogenase-like	Nsdhl	-0.6	-1	-2.2	93868_at
Pyruvate kinase liver and red blood cell	Pklr	-0.1	-0.5	-1.8	101471_at
Pyruvate kinase liver and red blood cell	Pklr	0.1	-0.4	-1.8	101472_s_at
Phosphomannomutase 1	Pmm1	0.2	0.6	-2	93360_at
Stearoyl-Coenzyme A desaturase 2	Scd2	-0.2	-0.8	-1.7	95758_at
Solute carrier family 2 (facilitated glucose transporter), member 2	Slc2a2	0	-0.3	-2.2	103357_at
Protein/amino acid metabolism					
Ankyrin 3, epithelial	Ank3	-0.4	-0.7	-1.9	98477_s_at
Archain 1	Arcn1	-1.9	0.6	-0.2	94512_f_at
Arginase 1, liver	Arg1	-0.1	-0.5	-1.9	93097_at
Dopa decarboxylase	Ddc	-0.2	-0.1	-2.5	160074_at
Ubiquitin-conjugating enzyme E2E 3, UBC4/5 homolog (yeast)	Ube2e3	0.5	3.2	3.8	93033_at
Cell cycle/apoptosis					
Cyclin F	Ccnf	0.2	0.4	-1.5	99073_at
Cyclin G1	Ccng1	0.2	1.3	2.2	160127_at
Growth arrest and DNA-damage-inducible 45 beta	Gadd45b	0.4	0.6	2.3	102779_at
Kinesin family member 2C	Kif2c	-0.3	0.9	2.1	160755_at
Lysyl oxidase	Lox	-1.5	0.3	0	161177_f_at
Moloney leukemia virus 10	Mov10	-0.2	-0.5	-1.5	103025_at
Myeloblastosis oncogene-like 1	Mybl1	0.2	0.6	1.7	92902_at
p53 apoptosis effector related to Pmp22	Perp	0	0.7	1.6	97825_at
Protein inhibitor of activated STAT 3	Pias3	0.7	0.8	1.7	160615_at
RAD51-like 1 (S. cerevisiae)	Rad51l1	-2.1	1.7	2.3	103944_at
SH3-domain GRB2-like B1 (endophilin)	Sh3glb1	0.3	-0.8	-1.8	103569_at
Serum-inducible kinase	Snk	0.9	0.7	2.3	92310_at
Serine/threonine kinase 6	Stk6	0.3	0.4	1.5	92639_at
Tumor necrosis factor receptor superfamily, member 6	Tnfrsf6	0.6	0.6	2	102921_s_at
Immune and inflammation					
Activated leukocyte cell adhesion molecule	Alcam	-0.4	-0.5	-2	104407_at
Amine oxidase, copper containing 3	Aoc3	0.4	0.4	1.7	102327_at
Chemokine (C-C motif) ligand 2	Ccl2	0.2	-0.9	-2.4	102736_at
Chemokine (C-C motif) ligand 7	Ccl7	0.3	-1	-1.9	94761_at
CD47 antigen (Rh-related antigen, integrin-associated signal transducer)	Cd47	0.2	-0.3	-1.5	103611_at
Complement component factor h	Cfh	-0.2	-0.6	-1.5	94743_f_at
Decay accelerating factor 1	Daf1	-2.5	0.2	2.4	103617_at
Insulin-like growth factor binding protein 1	Igfbp1	-0.2	-0.7	-1.6	103896_f_at
Lipopolysaccharide binding protein	Lbp	0.1	-0.5	-1.8	96123_at
Mannan-binding lectin serine protease 1	Masp1	-0.6	-0.4	-2	102284_at
Serum amyloid A 4	Saa4	0.3	0.2	1.5	92242_at
Thromboxane A synthase 1, platelet	Tbxas1	0.6	1.5	2.6	162136_r_at
Stress response and xenobiotic metabolism					
ATP-binding cassette, sub-family B (MDR/TAP), member 1B	Abcb1b	0.5	0	1.7	93414_at
Aldo-keto reductase family 1, member C6	Akr1c6	0.1	0.4	1.7	92556_at
Ceruloplasmin	Cp	-0.1	-0.8	-2	92851_at
Heat shock transcription factor 4	Hsf4	0	0.3	1.7	100384_at
Heat shock protein 1A	Hspa1a	0.3	0.3	2.7	93875_at
heat shock protein 1B	Hspa1b	-0.3	0.3	1.8	100946_at
Lactotransferrin	Ltf	0.7	1.7	3.2	101115_at
Solute carrier family 11 (proton-coupled divalent metal ion transporters), member 2	Slc11a2	-0.1	-0.5	-2.1	104451_at
Sulfotransferase family 1A, phenol-preferring, member 1	Sult1a1	-0.4	-0.8	-2	103087_at

Table 2. *(continued)*

Title	GeneName	1 mM 6 h	1 mM 24 h	3 mM 24 h	Affy ID
Cytoskelton etc.					
Cadherin 2	Cdh2	0.1	-0.2	-1.8	102852_at
Gap junction membrane channel protein alpha 1	Gja1	-0.2	0.2	-2.1	100065_r_at
Gap junction membrane channel protein beta 2	Gjb2	-0.2	-0.4	-2.1	98423_at
Gephyrin	Gphn	-0.9	0.1	-2.1	99441_at
Microtubule-actin crosslinking factor 1	Macf1	-1.7	0.3	0.1	98402_at
Microtubule-associated protein 4	Mtap4	0.1	-1	-1.6	92795_at
Par-3 (partitioning defective 3) homolog (C. elegans)	Pard3	-0.8	-0.3	-1.5	160607_at
p300/CBP-associated factor	Pcaf	0.2	-0.6	-1.8	161116_at
Ryanodine receptor 3	Ryr3	-0.6	-2.3	-2.5	97126_at
Stathmin 1	Stmn1	0.3	0.2	-1.5	97909_at
Utrophin	Utrn	-1.4	-0.5	-1.7	92507_at
Miscellaneous					
Betacellulin, epidermal growth factor family member	Btc	-0.3	-1.7	-0.9	95310_at
Creatine kinase, mitochondrial 1, ubiquitous	Ckmt1	-0.8	-0.3	1.7	160565_at
Procollagen, type IV, alpha 5	Col4a5	0.2	0	-2.2	93220_at
Cysteine rich protein 2	Crip2	0.3	0.4	1.8	101593_at
C-terminal binding protein 2	Ctbp2	-0.2	0	-3.8	160979_at
Fibroblast growth factor 1	Fgf1	0.2	-0.5	-1.7	100494_at
Fibroblast growth factor 7	Fgf7	0.1	-0.1	-1.9	99435_at
Gastric intrinsic factor	Gif	-0.2	1.2	1.7	92690_at
Homeo box A9	Hoxa9	-2	-0.7	0.4	92745_at
Hydroxysteroid (17-beta) dehydrogenase 2	Hsd17b2	0	-0.6	-1.5	101891_at
Inositol 1,4,5-triphosphate receptor 5	Itpr5	-1	-0.4	-1.7	101441_i_at
Male enhanced antigen 1	Mea1	0.5	2	0.6	94890_at
Matrix metalloproteinase 15	Mmp15	1.2	0.9	1.5	93612_at
Nemo like kinase	Nlk	-0.6	-0.4	-2.4	93935_at
Expressed in non-metastatic cells 4, protein	Nme4	-0.1	0.9	1.9	160473_at
Nicotinamide nucleotide transhydrogenase	Nnt	-0.1	-0.4	-1.7	99009_at
Paired box gene 6	Pax6	-0.4	2.8	3.2	92271_at
Protein phosphatase 2, regulatory subunit B (B56), delta isoform	Ppp2r5d	1.4	1	1.9	101875_at
DNA primase, p58 subunit	Prim2	0	-0.6	-3.2	95549_at
Platelet-activating factor receptor	Ptafr	-0.5	0.7	2	94158_f_at
Reelin	Reln	-2.6	-1.4	-1.7	96591_at
Serine (or cysteine) proteinase inhibitor, clade E, member 1	Serpine1	-0.5	-0.1	-1.9	94147_at
Serine (or cysteine) proteinase inhibitor, clade E, member 2	Serpine2	0.6	1.9	2.6	97487_at
Serine (or cysteine) proteinase inhibitor, clade F, member 2	Serpinf2	-0.2	-0.4	-1.8	101928_at
Splicing factor, arginine/serine-rich 1 (ASF/SF2)	Sfrs1	0.1	0.1	-2.5	160141_r_at
Sialyltransferase 9 (CMP-NeuAc:lactosylceramide alpha-2,3-sialyltransferase)	Siat9	-0.4	-0.6	-1.8	98596_s_at
Solute carrier family 25 (mitochondrial carrier; adenine nucleotide translocator), member 4	Slc25a4	0.3	-0.4	-1.5	93084_at
Small proline-rich protein 1B	Sprr1b	-0.2	2.5	1.3	100445_f_at
Endothelial-specific receptor tyrosine kinase	Tek	-1.5	0.2	0.6	102720_at
Troponin C, cardiac/slow skeletal	Tncc	0.4	0.4	1.7	101063_at
Urate oxidase	Uox	-0.1	-0.5	-2	92606_at

Data is shown as signal $\log_2$ ratio to each control group.

related to Pmp22' (perp). Thus, the activation of apoptosis should be envisioned. These expression changes should be related to the compaction and margination of nuclear chromatin.

Many genes related to lipid and glucose metabolism were down-regulated. Some of the fatty acid synthesis-related factors, 'stearoyl-CoA desaturases' (Scd1, Scd2) and 'fatty acid syhthase' (fasn), and cholesterol synthetase, '3-hydroxy-3-methylglutaryl-Coenzyme A synthase 1' (Hmgcs1) were down-regulated. 'Mttp', which transfers lipids onto the apoB polypeptide in the endoplasmic reticulum (Raabe et al., 1999), was also down-regulated. We observed similar results in vivo (Kume et al., in press). These findings may not indicate that SZ controls these parameters directly, but may indicate that the energy for the lipid and glucose metabolism was not supplied due to the hepatocyte injury.

Most of the genes related to the stress-response and xenobiotic metabolism such as 'RAD51-like 1' (Rad51l1) and 'Heat shock transcription factor 4'

Table 3. Gene expressions in primary cultured hepatocytes exposed with SZ (in vitro) and in the SZ-treated mice (in vivo)

GeneName	*in vitro* 3 mM 24 h	*in vivo* 200 mg/kg 24 h	AffyID
Carbohydrate and lipid metabolism			
Amy2	-1.4	-0.5	97523_i_at
Clps	-0.1	-2.1	160132_at
Clo1	-1.5	-1.9	103581_at
Cyp51	-1.7	-2.2	94916_at
Cyp8b1	-1.2	-3.6	103284_at
Fabp1	-1.8	-0.7	94075_at
Fasn	-0.8	-1.5	98575_at
Fdps	-1	-2	160424_f_at
Fdps	-0.8	-2.8	99098_at
Gck	-1.9	-2.4	102651_at
Hmgcs1	-1.5	-1.5	94325_at
Hmgcs2	-2.1	-2.1	92590_at
Idi1	-1.5	-2.5	96269_at
Lipc	-0.5	-1.9	98962_at
Mttp	-1.7	-0.1	104448_at
Nsdhl	-2.2	-1.8	93868_at
Nsdhl	-1.5	-1.7	98631_g_at
Pldr	-1.8	-1.2	101471_at
Pldr	-1.8	-0.5	101472_s_at
Pmm1	-2	-3.9	93360_at
Pnliprp1	-2.7	-1.4	92601_at
Sc4mol	-0.3	-2	160388_at
Scd1	-0.5	-1.7	94057_g_at
Scd2	-1.7	-0.1	95758_at
Slc2a2	-2.2	-0.3	103357_at
Thrsp	0.7	-1.7	160306_at
Protein/amino acid metabolism			
Ank3	-1.9	-1.4	98477_s_at
Arg1	-1.9	-0.4	93097_at
Bhmt	-0.2	-1.9	94049_at
Csad	-0.7	-2.4	99184_at
Ddc	-2.5	-1.3	160074_at
Ela1	0.5	-1.7	93783_at
Fbxo21	-0.3	-1.7	104109_at
Gamt	0.8	-2	101408_at
Mug1	-1.2	-1.6	92837_f_at
Tat	-0.5	-1.9	96326_at
Try4	-1.4	-2.2	101043_f_at
Ube2e3	-1.9	0.2	93033_at

GeneName	*in vitro* 3 mM 24 h	*in vivo* 200 mg/kg 24 h	AffyID
Cell cycle/apoptosis			
Bax	0.8	-1.7	93536_at
Btg2	0.7	-2.2	101593_at
Ccnf	-1.6	0.3	99073_at
Ccng1	-2.2	-3	160127_at
Cdkn1a	-1.2	-2.7	94881_at
Cdkn1a	-1.4	-3.6	98067_at
Dusp6	-1	-1.8	93285_at
Ei24	0.9	-1.5	99629_at
G0s2	0	-1.5	97531_at
Gadd45b	-2.2	0.9	102779_at
Kif2c	-2.4	0.2	160755_at
Lox	0	-1.6	161177_f_at
Mdm2	-1.4	-2.6	98110_at
Mov10	-1.5	-0.2	103025_at
Mybl1	-1.7	-2.1	92902_at
Perp	-1.7	-1.8	97825_at
Pias3	-1.7	-2.4	160615_at
Sh3glb1	-1.8	0	103569_at
Snk	-2.3	-1.8	92310_at
Stk6	-1.5	-0.3	92639_at
Tnfrsf6	-2	-1.6	102921_s_at
Tob1	0.2	-1.5	99532_at
Wig1	0.9	-1.8	92262_at

GeneName	*in vitro* 3 mM 24 h	*in vivo* 200 mg/kg 24 h	AffyID
Stress response and xenobiotic metabolism			
Abcb1b	-1.7	-3.2	93414_at
Akr1c6	-1.7	-0.5	92556_at
Cp	-2	-0.7	92851_at
Cyp2b9	-0.1	-3.8	101882_at
Fmo3	-0.8	-1.7	104421_at
Hsf4	-1.7	-2.8	100384_at
Hspa1a	-2.7	-0.8	93875_at
Hspa1b	-1.9	-1.5	100946_at
Ltf	-6.2	-1	101115_at
Rad51l1	-2.3	0.2	103944_at
Saa3	0.3	-2	102712_at
Slc11a2	-2.1	-1.1	104451_at
Sult1a1	-2	-0.4	103087_at
Temt	-1.1	-3.3	97402_at
Txnl2	-1	-1.6	95696_at
Immune and inflammation			
Alcam	-2	-1	104407_at
Aoc3	-1.7	-0.4	102327_at
Arhb	-0.3	-1.7	101030_at
Ccl2	-2.4	-2.2	102736_at
Ccl7	-1.9	-1.3	94761_at
Cd47	-1.5	-0.2	103611_at
Cfh	-1.5	0	94743_f_at
Cxcl1	-0.9	-1.7	95348_at
Cxcl1	-0.8	-2	95349_g_at
Cxcl12	0.2	-1.5	100112_at
Daf1	-2.1	0.2	103617_at
Icam1	0.6	-2	96752_at
Igfbp1	-1.6	0.2	103896_i_at
Lbp	-1.8	-1.2	96123_at
Ly6d	0.5	-1.9	160553_at
Masp1	-2	-0.9	102284_at
Mbl2	0.7	-2	97427_at
Nfe2l2	-0.4	-1.9	92562_at
Pigr	0	-1.7	99926_at
S100a11	0.1	-1.7	98600_at
Saa4	-1.9	0.3	92242_at
Serpina6	0.3	-2.4	96227_at
Tbxas1	-2.6	-2.7	162136_r_at

GeneName	*in vitro* 3 mM 24 h	*in vivo* 200 mg/kg 24 h	AffyID
Miscellaneous			
Ahcy	-0.1	-1.5	98024_at
Alas2	-1.5	-0.2	92768_s_at
Ang	0.7	-1.6	94302_f_at
Atp6v1d	0.7	-2.6	96851_at
Car14	-0.2	-1.6	98079_at
Car3	0.9	-2.3	160375_at
Car5a	0.7	-1.7	98137_at
Ccrn4l	-0.1	-1.6	99535_at
Cdh2	-1.8	-0.2	102852_at
Ckmt1	-1.7	-2.5	160565_at
Col4a5	-2.2	-0.6	93220_at
Crip2	-1.6	-1	101593_at
Cttbp2	-3.8	0.2	160979_at
Dbp	0.7	-3.3	160841_at
Dio1	-0.3	-1.8	95552_at
Fgf1	-1.7	-1.4	100494_at
Fgf7	-1.6	0.4	99435_at
Gif	-1.7	-0.1	92690_at
Gja1	-2.1	-0.3	100065_r_at
Gjb2	-2.1	-0.6	98423_at
Gphn	-2.1	-0.6	99441_at
Hsd17b2	-1.5	-1.3	101891_at
Igfbp2	0	-2.2	98627_at
Ilpr5	-1.7	-0.3	101441_i_at
Klk6	-1.7	-1.6	100061_f_at
Lpin1	-0.4	-1.6	98892_at
Mmp15	-1.6	-0.2	93612_at
Mtap4	-1.6	-0.6	92795_at
Nlk	-2.4	0.1	93935_at
Nme4	-1.4	-1.4	160473_at
Nnt	-1.7	-0.5	99009_at
Pard3	-1.5	-0.7	160607_at
Pax6	-2.2	-0.2	92271_at
Pcaf	-1.8	-0.2	161116_at
Ppp2r5d	-1.9	-0.2	101875_at
Prim2	-3.2	-2.1	95549_at
Ptafr	-2	0.1	94158_f_at
Reln	-1.7	-0.7	96591_at
Ren1	-1.7	-1.2	98480_s_at
Ryr3	-2.5	-0.1	97126_at
Scn1b	0.8	-2.6	102808_at
Serpine1	-1.9	-2.1	94147_at
Serpine2	-2.6	0.8	97487_at
Serpinf2	-1.8	-0.4	101928_at
Sfrs1	-2.5	-1.6	160141_r_at
Siat9	-1.8	0.6	98596_s_at
Slc25a4	-1.5	0.6	93084_at
Sprr1b	-2.3	0.5	100445_f_at
Stmn1	-1.5	-1.1	97909_at
Tek	0.6	-2.2	102720_at
Tncc	-1.7	-2.7	101063_at
Uox	-2	-0.8	92606_at
Utrn	-1.7	0.8	92507_at

Data is shown as signal $\log_2$ ratio to each control group.

(Hsf4) were up-regulated in vitro and in vivo. However, some genes related to the stress-response such as 'heat shock proteins' (Hspa1a, 1b) were up-regulated in vitro but not in vivo. Those proteins directly related to the nuclear damages, i.e. Rad51l1 and Hsf4, might be regulated the same in vitro and in vivo, and some genes in this category, such as hspa1a and 1b, might be regulated in a more complicated manner.

The most conspicuous difference was observed in the immune/allergy related genes. In the other categories, most genes were regulated in the same direction, but many of the immune/allergy-related genes were regulated in the opposite direction between in vivo and in vitro. Most genes were up-regulated in vivo, although in vitro most were down-regulated. The reason is unknown, but it could be related to the fact that there were practically no immune cells interacting with hepatocytes in the in vitro condition.

We can see the similarity in directions for the gene expression changes in 1 mM-24 h exposure group and 3 mM-24 hr exposure group, although the magnitudes were different. Only four genes in the tabulated 95 genes were regulated in opposite directions. Therefore, we can say that the gene expression changes were dose dependent, and small changes, i.e.—$1.0 < SLR < 1.0$, should have had some meaning. We should pay attention to those small expression changes.

In conclusion, SZ induced morphological and gene expression changes in vitro. Those changes were related to apoptosis, cell proliferation, and carbohydrate and lipid metabolisms, and were similar as those observed in vivo. These results strongly support the former results; those changes, which started prior to the elevation of the serum glucose levels, were due to the direct action of SZ on the liver, rather than the secondary effect of diabetes.

Acknowledgements

We thank Ms H. Yamasaki, Ms M. Kurabe, Ms E. Ohtsuka, Ms N. Shimazu, and other members of our laboratory for their technical assistance.

Reference

Bellmann K, Wenz A, Radons J, Burkart V, Kleemann R, Kolb H. Heat shock induces resistance in rat pancreatic islet cells against nitric oxide, oxygen radicals and streptozotocin toxicity in vitro. J Clin Invest 1995;95: 2840–5.

Bhuyan BK. The action of streptozotocin on mammalian cells. Cancer Res 1970;30:2017–23.

Capucci MS, Hoffmann ME, De Groot A, Natarajan AT. Streptozotocin-induced toxicity in CHO-9 and V79 cells. Environ Mol Mutagen 1995;26:72–8.

Doi K, Yamanouchi J, Kume E, Yasoshima A. Morphologic changes in hepatocyte nuclei of streptozotocin (SZ)-induced diabetic mice. Exp Toxic Pathol 1997;49:295–9.

Eizirik DL, Bjorklund A, Cagliero E. Genotoxic agents increase expression of growth arrest and DNA damage—inducible genes gadd 153 and gadd 45 in rat pancreatic islets. Diabetes 1993;42:738–45.

Flament P, Remacle C. Ultrastructural aspects of streptozotocin cytotoxicity on rat pancreatic islets in vitro. Virchows Arch B 1987;53:107–12.

Kume E, Doi C, Itagaki S, Nagashima Y, Doi K. Glomerular lesions in unilateral nephrectomized and diabetic (UN-D) mice. J Vet Med Sci 1992;54:1085–90.

Kume E, Itagaki S, Doi K. Cytomegalic hepatocytes and bile duct hyperplasia in streptozotocin-induced diabetic mice. J Toxicol Pathol 1994a;7:261–5.

Kume E, Ohmachi Y, Itagaki S, Tamura K, Doi K. Hepatic changes of mice in the subacute phase of streptozotocin (SZ)-induced diabetes. Exp Toxic Pathol 1994b;46:368–74.

Kume E, Fujimura H, Matsuki N, Ito M, Aruga C, Toriumi W, Kitamura K, Doi K. Hepatic changes in the acute phase of streptozotocin (SZ)-induced diabetes in mice. Exp Toxic Pathol 2004;55:467–80.

Kume E, Aruga C, Takahashi K, Miwa S, Ito M, Fujimura H, Toriumi W, Kitamura K, Doi K. Gene expression profiling in streptozotocin treated mouse liver using DNA microarray. Exp Toxic Pathol, in press.

Ledoux SP, Wilson GL. Effects of streptozotocin on a clonal isolate of rat insulinoma cells. Biochim Biophys Acta 1984;804:387–92.

Raabe M, Veniant MM, Sullivan MA, Zlot CH, Bjorkegren J, Nielsen LB, Wong JS, Hamilton RL, Young SG. Analysis of the role of microsomal triglyceride transfer protein in the liver of tissue-specific knockout mice. J Clin Invest 1999;103:1287–98.

Sibay TM, Hausler HR, Hayes JA. The study and effect of streptozotocin (NSC-37917) rendered diabetic chinese hamsters. Ann Ophthalmol 1971;3:596–601.

Steffes MW, Mauer SM. Diabetic glomerulopathy in man and experimental animal models. Int Rev Exp Pathol 1984;26: 147–75.

Turk J, Corbett J A, Ramanadham S, Bohrer A, Mcdaniel ML. Biochemical evidence for nitric oxide formation from streptozotocin in isolated pancreatic islets. Biochem Biophys Res Commun 1993;197:1458–64.

Wang K, Shindoh H, Inoue T, Horii I. Advantages of in vitro cytotoxicity testing by using primary rat hepatocytes in comparison with established cell lines. J Toxicol Sci 2002;27:229–37.

J Pharmacol Sci 103, 48 – 55 (2007)

Journal of Pharmacological Sciences

Full Paper

Role of Mouse Organic Anion Transporter 3 (mOat3) as a Basolateral Prostaglandin E_2 Transport Pathway

Sirinun Nilwarangkoon[1], Naohiko Anzai[1], Katsuko Shiraya[1], Erkang Yu[1], Rafiqul Islam[1], Seok Ho Cha[1], Maristela Lika Onozato[2], Daisaku Miura[1], Promsuk Jutabha[1], Akihiro Tojo[2], Yoshikatsu Kanai[1], and Hitoshi Endou[1,*]

[1]*Department of Pharmacology and Toxicology, Kyorin University School of Medicine, 6-20-2 Shinkawa, Mitaka, Tokyo 181-8611, Japan*
[2]*Department of Nephrology and Endocrinology, University of Tokyo, 7-3-1, Hongo, Bunkyo-ku, Tokyo 113-8655, Japan*

Received July 24, 2006; Accepted November 14, 2006

Abstract. Renal organic anion transporters play an important role in the handling of a number of endogenous and exogenous anionic substances in the kidney. In this study, we investigated prostaglandin E_2 (PGE_2) transport properties and intrarenal localization of mouse organic anion transporter 3 (mOat3). When expressed in *Xenopus* oocytes, mOat3 mediated the time- and concentration-dependent transport of PGE_2 (K_m: 1.48 μM). PGE_2 transport mediated by mOat3 was *trans*-stimulated by intracellular glutarate injected into the oocytes. PGE_2 efflux via mOat3 was also *trans*-stimulated by extracellular glutarate. Thus, mOat3 was shown to mediate the bidirectional transport of PGE_2, partly coupled to the dicarboxylate exchange mechanism. Immunohistochemical study revealed that mOat3 protein was localized at the basolateral membrane of renal proximal and distal tubules. Furthermore, diffuse expression of mOat3, including expression in the basolateral membrane in macula densa (MD) cells, was observed. These results indicate that mOat3 plays an important role as a basolateral transport pathway of PGE_2 in the distal nephron including MD cells that may constitute one of the indispensable steps for renin release and regulation of the tubuloglomerular feedback mechanism.

Keywords: organic anion transporter, OAT, prostaglandin E_2, glutarate, macula densa

Introduction

Prostanoids, which include prostaglandins (PGs) and thromboxanes (TXs), are cyclooxygenase (COX)-dependent metabolites of arachidonic acids and play various physiological and pathophysiological roles (1, 2). Among them, PGE_2 is the major prostanoid in the kidney and is synthesized at high rates along the nephron, particularly in the collecting duct (3). PGE_2 plays an important role in the tubular reabsorption of salt and water as well as in the control of renal vascular resistance and the maintenance of glomerular hemodynamics. In addition, PGE_2 stimulates the release of renin from the juxtaglomerular apparatus (JGA). Recently, it has been reported that intact macula densa (MD) cells synthesize and release PGE_2 when luminal salt content is reduced, and it has been suggested that this response is involved in the control of renin release and renal vascular resistance during salt deprivation (4). In these functions, PGE_2 mediates autocrine and paracrine signaling over short distances through the activation of its four receptor subtypes (EP_1, EP_2, EP_3, and EP_4) (3). Thus, to maintain the extracellular concentration of PGE_2, the termination of PGE_2 signaling requires rapid re-uptake of released PGE_2 followed by cytoplasmic oxidation (5). Since PGE_2 possesses anionic moieties at physiological pH and diffuses poorly through the lipid bilayer, it is thought that PGE_2 transport across the plasma membrane is a carrier-mediated transport process (5). However, little is known about the molecular mechanism of the release of PGE_2 in distal nephron including MD cells.

To date, several PG carriers have been characterized (5). Prostaglandin transporter PGT (Slc21a2, oatp2A1)

*Corresponding author. endouh@kyorin-u.ac.jp
Published online in J-STAGE: January 13, 2007
doi: 10.1254/jphs.FP0060816

is broadly expressed in COX-positive cells and is coordinately regulated with COX. By analogy with neurotransmitter release and re-uptake, PGT may regulate pericellular PG levels via re-uptake (6). Immunocytochemical study has revealed that PGT in rat kidneys was expressed in glomerular endothelial and mesangial cells, arteriolar endothelial and muscularis cells, principal cells of the collecting duct, medullary interstitial cells, and the medullary vasa rectae endothelia (7). In the collecting duct, PGT is expressed in subapical vesicles. These results indicate that PGT is unlikely to be involved in the basolateral transport of PGE_2 in distal nephron including MD cells. Certain PGs are actively extruded from cells by multidrug resistance-associated proteins (MRPs) (5); these may play a role in metabolic clearance of PGs. However, the expression of MRPs in MD cells is still unclear.

Organic anion transporter (OAT) family members are other PG transporters (8). OATs play important roles in the elimination of a variety of endogenous substances, xenobiotics and their metabolites, many of which are potentially toxic to the body (9 – 14). Recently, cDNAs encoding OAT family members, including OAT1, OAT2, OAT3, OAT4, URAT1 (urate transporter 1), and Oat5, have been successively cloned (9). Among these clones, OAT1(human)/Oat1(rodents) and OAT3/Oat3 were shown to be localized to the basolateral side of the proximal tubule, whereas OAT4, URAT1, and Oat5 were shown to be localized to the apical side of the proximal tubule. In contrast, the exact localization of OAT2 protein in the kidney is still controversial: Rat Oat2 was formerly identified at the apical membrane of the thick ascending limb of Henle and cortical collecting ducts (15), but recently it has been shown to be localized at the apical side of proximal straight tubules (S_3 segment) (16), whereas human OAT2 was found to be localized to the basolateral membrane of the proximal tubule (17).

Among the OATs, OAT3 protein expression was detected in nearly all of the nephron segments in the rat kidney (15). Thus, OAT3 is likely to be a transporter responsible for the basolateral transport of PGE_2 in distal nephron including MD cells. Although Oat3 knockout mice have been generated several years ago (18), information on the functional properties of mouse Oat3 (mOat3) is limited (19 – 21). In this study, we examined PGE_2 transport properties and intrarenal localization of mOat3.

Materials and Methods

Materials

The materials used in this study were purchased from the following sources: [^{14}C]*p*-aminohippurate (PAH) (1.90 GBq/mmol) was from Moravek Biochemicals (Brea, CA, USA); [^{3}H]estrone-3-sulfate (E_1S) (2.0 TBq /mmol), [^{14}C]glutarate (2.035 GBq/mmol), and [^{3}H]PGE_2 (7.429 TBq/mmol) were from PerkinElmer Life Science Products (Boston, MA, USA); and glutarate was from Wako (Osaka). All other chemicals and reagents used were of analytical grade and obtained from commercial sources.

Animals

Six-week-old male ICR mice were purchased from Saitama Experimental Animal Co., Ltd. (Saitama) and kept under routine laboratory conditions with free access to standard laboratory chow and water.

Isolation of mOat3

A nondirectional cDNA library for screening was prepared from mouse kidney poly(A)$^-$ RNA using a Superscript Choice System (Invitrogen, Carlsbad, CA, USA) and was ligated into the phage vector ZipLox EcoRI arms (Invitrogen). The library was screened by homology using full-length rOat3 cDNA labeled with [^{32}P]dCTP by random priming (T7Quick Prime Kit; Amersham Pharmacia Biotech, Uppsala, Sweden) as a probe as described previously (22). cDNA inserts in positive ZipLox phages were recovered in the plasmid pZL1 vector by in vitro excision and completely sequenced with specially synthesized oligonucleotide primers by the dye terminator method using an ABI 3100 Genetic Analyzer (Applied Biosystems, Foster City, CA, USA).

cRNA synthesis and uptake experiments using Xenopus laevis oocytes

cRNA synthesis and uptake experiments were performed as described previously (23). The capped cRNA of mOat3 was synthesized in vitro by T7 RNA polymerase from a plasmid linearlized with Xba I. Defolliculated oocytes were injected with 10 ng of the capped mOat3 cRNA or water (control) and incubated in Barth's solution (88 mM NaCl, 1 mM KCl, 0.33 mM $Ca(NO_3)_2$, 0.4 mM $CaCl_2$, 0.8 mM $MgSO_4$, 2.4 mM $NaHCO_3$, and 10 mM HEPES) containing 50 μg/ml gentamicin at 18°C. After 2 to 3 days of incubation, uptake experiments of radiolabeled substrates, as indicated in each experiment, were performed at room temperature in ND96 solution (96 mM NaCl, 2 mM KCl, 1.8 mM $CaCl_2$, 1 mM $MgCl_2$, and 5 mM HEPES, pH 7.4). Each experiment was repeated more than two times to confirm the results. Representative results are shown in the figures.

Kinetic parameter for the uptake of PGE_2 via mOat3

was estimated from the following equation: $v = (V_{max} \times S) / (K_m + S)$, where v is the rate of substrate uptake (pmol/h·oocyte), S is the substrate concentration in the medium (μM), K_m is the Michaelis-Menten constant (μM), and V_{max} is the maximum uptake rate (pmol/h·oocyte). These kinetic parameters were determined with the Eadie-Hofstee equation.

To examine the *trans*-stimulatory effects of both the uptake and efflux of radiolabeled substrates, cold glutarate (50 mM) (Fig. 3) or 50 nl of [^{3}H]PGE_2 (0.6 μM) (Fig. 4) was injected into oocytes expressing mOat3 with a fine-tipped glass micropipette as described previously (24). Then individual oocytes were washed twice with ice-cold ND96 solution, placed on ice for 5 min, then incubated with ND96 at room temperature for 1 h, and finally transferred into a medium with or without radiolabeled E_1S (Fig. 3A) or PGE_2 (Fig. 3B) or with cold glutarate (10 mM) (Fig. 4) and incubated at room temperature for 1 h. [^{3}H]PGE_2 before and after taken up by the oocytes was little degraded as Chan et al. reported previously (25). Radioactivity in both the medium and oocytes was determined after a 1-h incubation.

For the uptake and efflux measurements in the present study, 8 – 10 oocytes were used for each data point. The values are expressed as means ± S.E.M. Each experiment was repeated at least twice to confirm the results. Results from representative experiments are shown in the figures.

Immunohistochemical analysis

For immunohistochemical analysis, rabbits were immunized with a keyhole limpet hemocyanin-conjugated synthesized peptide, CKASQTIPLKTGDPS, corresponding to cysteine and the 14 amino acids of the COOH terminus of mOat3. Two-micrometer wax sections of nephrectomized mouse kidney were processed for light microscopic immunohistochemical analysis using the streptavidin-biotin-horseradish peroxidase complex technique (LSAB kit; DAKO, Carpinteria, CA, USA). Sections were dewaxed, rehydrated, and incubated with 3% H_2O_2 for 10 min to eliminate endogenous peroxidase activity. After rinsing in 0.05 M Tris-buffered saline containing 0.1% Tween-20, sections were treated with 10 μg/ml of primary rabbit polyclonal antibody (at 4°C overnight). Thereafter, the sections were incubated with the secondary antibody, biotinylated goat polyclonal antibody against rabbit immunoglobulin (DAKO), diluted 1:400 for 30 min with horseradish peroxidase-labeled streptavidin. This step was followed by incubation with diaminobenzidine and hydrogen peroxide. The sections were counterstained with hematoxylin and examined by light microscopy. For a preabsorption experiment, the mOat3 peptide (200 μg/ml) was added to the mOat3-specific antibody solution and incubated overnight at 4°C. Using this preabsorbed antibody, immunohistochemistry was performed as described above.

Statistical analysis

Data are expressed as means ± S.E.M. Statistical differences were determined using Student's *t*-test. The reproducibility of the results in the present study was confirmed using two or three separate experiments. Results from representative experiments are shown in the figures.

Results

mOat3 cDNA was isolated from the kidney. As shown in Fig. 1, mOat3 mediated the transport of [^{14}C]PAH, [^{3}H]E_1S, [^{3}H]glutarate, and [^{3}H]PGE_2. These results indicate that our mOat3 clone is functional and its transport activity is compatible with that reported previously (18 – 20).

The uptake by mOat3 cRNA-injected oocytes increased linearly for about 180 min (Fig. 2A). Accord-

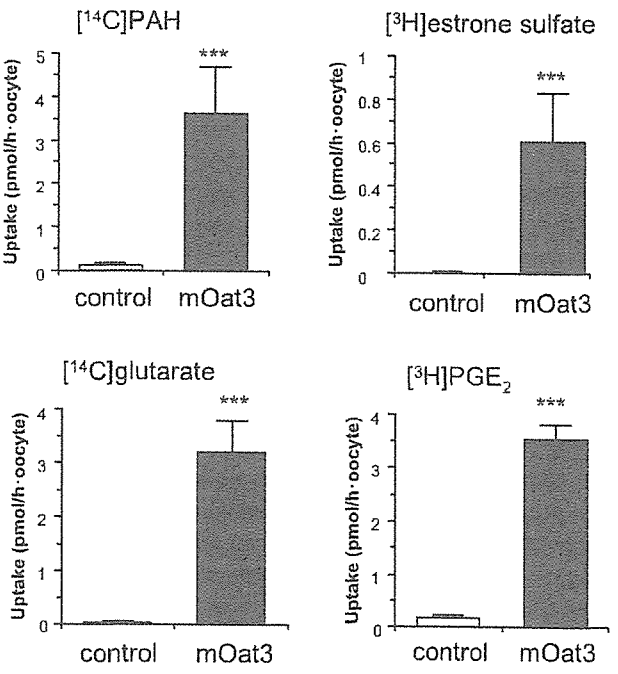

Fig. 1. Functional expression of mOat3 in *Xenopus* oocytes. mOat3 mediated the transport of several organic anions. The uptakes of radiolabeled [^{14}C]*p*-aminohippurate (PAH) (12 μM), [^{3}H]estrone sulfate (55 nM), [^{14}C]glutarate (5.5 μM), and [^{3}H]prostaglandin E_2 (PGE_2) (5 nM) by water-injected control oocytes and by mOat3-expressing oocytes were determined over a period of 1 h (mean ± S.E.M., n = 8 – 10). ***P<0.001 versus control.

ingly, analysis was performed at 60 min in the following experiments. The concentration dependence of the uptake of [^{3}H]PGE_2 via mOat3 is shown in Fig. 2B. The mOat3-mediated [^{3}H]PGE_2 uptake showed saturable kinetics and could be modeled by the Michaelis-Menten equation. Eadie-Hofstee plot analyses yielded a K_m value of 1.48 μM for PGE_2.

It is well established that OAT1 is a classical PAH /dicarboxylate exchanger (9). In addition, Sweet et al. and Bakhiya et al. reported that rat and human Oat3 /OAT3 functions as an organic anion/dicarboxylate exchanger (26, 27). Given the high sequence identity between rat Oat3 and mOat3, we assumed that their functions are very similar. However, a recent study by Ohtsuki et al. failed to demonstrate the E_1S/dicarboxylate exchange mechanism in mOat3 (19). Therefore, we next examined whether mOat3 is also organic anion /dicarboxylates exchanger or not. The uptake of [^{3}H]E_1S via mOat3 was *trans*-stimulated by the injection of cold glutarate into the oocytes (Fig. 3A). In addition, mOat3 mediated PGE_2/dicarboxylate exchange (Fig. 3B). We conclude that mOat3, as well as rat and human Oat3/OAT3, functions as an organic anion/dicarboxylate exchanger.

Then we examined the efflux of [^{3}H]PGE_2 from oocytes expressing mOat3. mOat3 exhibited significant efflux for [^{3}H]PGE_2, compared with water-injected

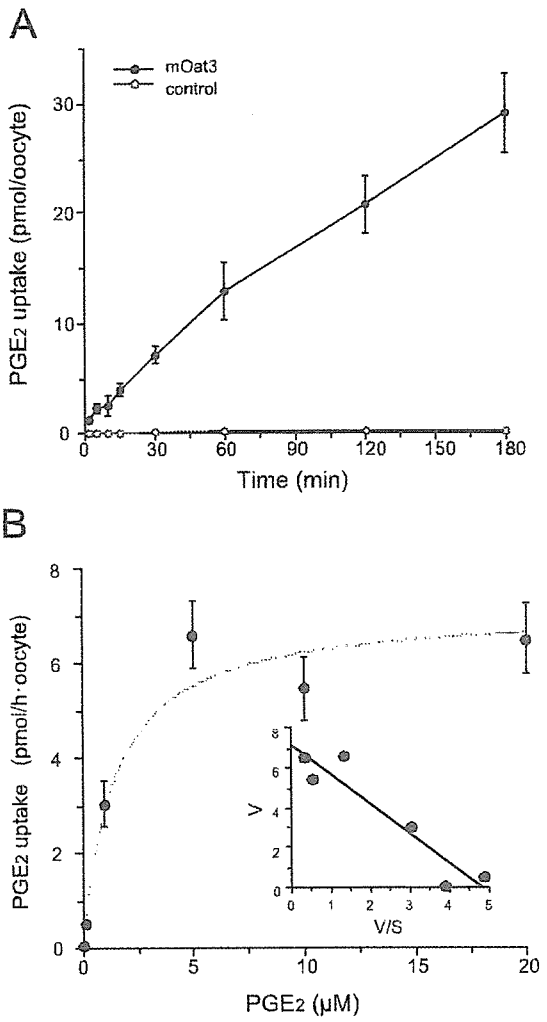

Fig. 2. Transport properties of PGE_2 via mOat3. A: Time-dependent uptake of [^{3}H]PGE_2 via mOat3. The uptake of 5 nM [^{3}H]PGE_2 was measured for 3 h in control oocytes and oocytes expressing mOat3 (mean ± S.E.M., n = 8 – 10). B: Concentration-dependence of mOat3-mediated uptake of PGE_2. The uptake rate of PGE_2 by control or mOat3-expressing oocytes for 1 h was measured at various concentrations (mean ± S.E.M., n = 8 – 10). Inset: Eadie-Hofstee plot. V, velocity; V/S, velocity per concentration of PGE_2.

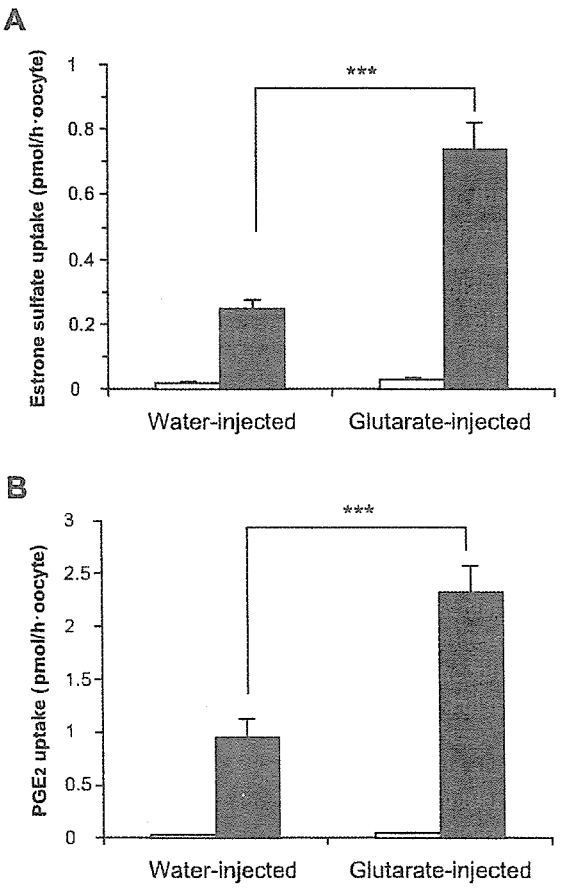

Fig. 3. Effects of glutarate on mOat3-mediated transport. *Trans*-stimulatory effect of glutarate on the uptake of [^{3}H]estrone sulfate (ES) (A) or [^{3}H]PGE_2 (B) via mOat3. Control (open column) and mOat3-expressing oocytes (closed column) were injected with 50 mM unlabeled glutarate (right columns) or water (left columns) and incubated for 5 min on ice. Then the oocytes were incubated with [^{3}H]ES (100 nM) or [^{3}H]PGE_2 (5 nM) and the amount of [^{3}H]ES or [^{3}H]PGE_2 accumulated for 1 h was determined (mean ± S.E.M., n = 8 – 10). ***P<0.001.

control oocytes (Fig. 4, left two columns). In addition, as would be expected for an exchanger, [^{3}H]PGE_2 efflux via mOat3 was significantly *trans*-stimulated by unlabeled glutarate in the medium (10 mM) (Fig. 4, right two columns).

Among the OAT isoforms, OAT3 as well as OAT1 are known to be polyspecific organic anion transporters that are responsible for the basolateral uptake of various organic anions (9 – 14). Although functional analysis of an Oat3 knockout mouse model strongly suggested that murine Oat3 was present in the basolateral membrane of renal proximal tubular cells (18), its exact localization in the kidney has not been demonstrated yet. Therefore, to clarify the intrarenal localization, we raised an antibody against the mOat3 C-terminal region and performed immunohistochemical analysis.

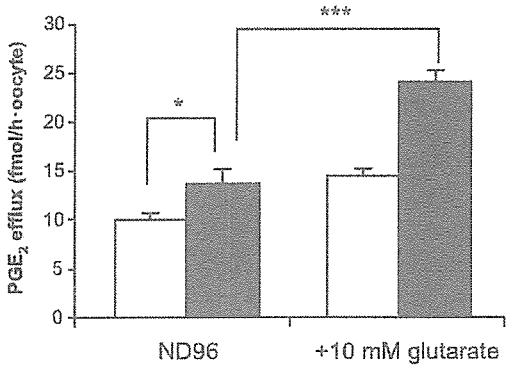

Fig. 4. mOat3-mediated butyrate efflux. *Trans*-stimulatory effect of glutarate on the efflux of [^{3}H]PGE_2 via mOat3. Control (open column) and mOat3-expressing (closed column) oocytes were injected with [^{3}H]PGE_2. After washing, the oocytes were incubated with 10 or 0 mM unlabeled glutarate. The amount of [^{3}H]PGE_2 effluxed for 1 h was determined. *P<0.05, ***P<0.001.

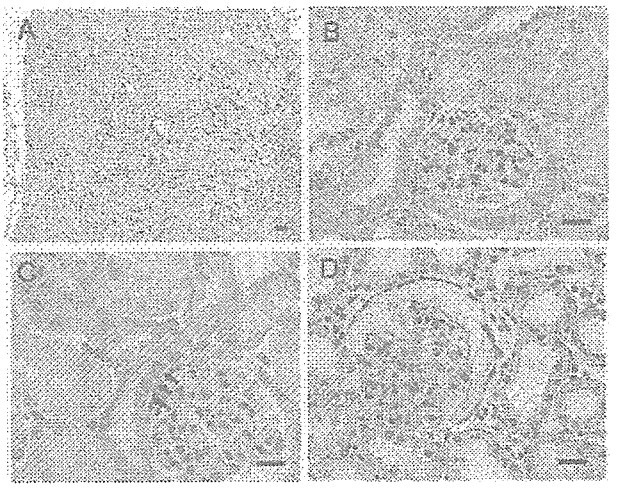

Fig. 5. Immunohistochemical analysis of Oat3 in mouse kidney. Two-micrometer sections were incubated with a polyclonal antibody against mOat3. Basolateral membrane of proximal tubules and that of distal tubules and collecting ducts were stained (proximal < distal), and no staining was observed in the glomeruli. Immunoreactivity in macula densa was also observed (arrows) at the basolateral side as well as the cytoplasm. (400×). Scale bars = 150 μm for A, 20 μm for B to D.

As shown in Fig. 5A, broad immunoreactivities of mOat3 were observed throughout the cortex under low magnification. There was no staining in the glomerulus. Under high magnification, mOat3 was found to be localized not only at the basolateral membrane of the proximal tubules but also at the same side of the distal tubules and of the collecting ducts (Fig. 5B). Interestingly, the intensities of mOat3 immunoreactivity seem stronger in the distal tubules and collecting ducts than in the proximal tubules. In addition, mOat3 immunoreactivity was detected in MD cells (Fig. 5C). By preincubation of the antibody with mOat3 peptide, the immunoreactivity disappeared (Fig. 5D). The specificity of the antibody for mOat3 was verified by these results.

Discussion

In this study, we analyzed mOat3-mediated PGE_2 transport properties and the intrarenal localization of mOat3 to determine whether mOat3 contributes to the basolateral transport of PGE_2 in distal nephron including MD cells.

PGE_2 is a major prostanoid derived from COX metabolism and modulates salt and water homeostasis in the kidney. In the renal cortex, COX-1 expression predominates in the collecting duct, vascular tissue, and glomerular mesangial cells, while COX-2 is expressed and presumably mediates PG production in the MD and surrounding cortical thick ascending limb (cTAL) cells (28 – 31). MD cells are in direct contact with the vascular pole of the same glomerulus from which the filtrate originates. They sense changes in tubular NaCl concentration and send signals to control preglomerular vascular resistance and glomerular filtration rate in a process named tubuloglomerular feedback (TGF). MD cells also control the renin release from juxtaglomerular granular cells (28 – 30). COX-2-derived PGs may participate in MD-mediated control of juxtaglomerular function, particularly in high renin states such as low salt intake, loop diuretic treatment, and renovascular hypertension (29, 31). PGE_2 produced by MD cells has been suggested to be the mediator of renin release induced by low luminal NaCl concentration (30 – 36). In addition, PGE_2, as a potent vasodilator, may also modulate preglomerular vascular resistance (3, 37) and TGF (38). Recently, it has been reported that PGE_2 release from MD cells is important in the control of renin release and

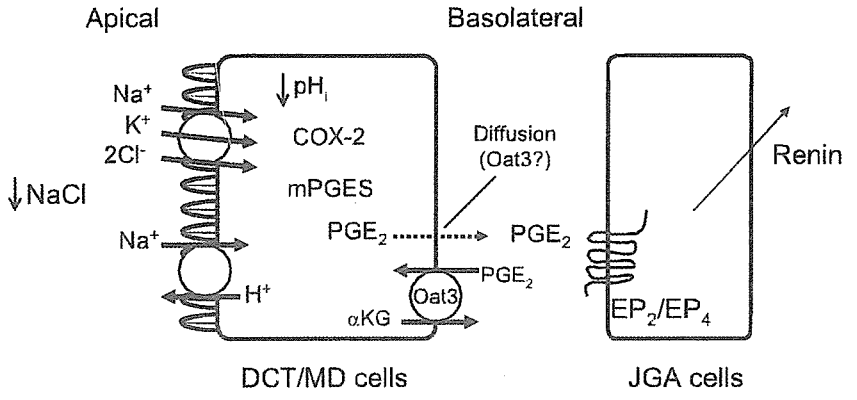

Fig. 6. Model of macula densa (MD) signaling. A marked decrease in tubular NaCl concentration, particularly under low salt diet, causes activation of the PG-synthesizing machinery, including COX-2 and microsomal PGE_2 synthase (mPGES) and PGE_2 release across the basolateral membrane via diffusion (or by Oat3). Oat3 is likely to be a transporter responsible for the rapid re-uptake of released PGE_2 using the outwardly directed gradient of dicarboxylates such as α-ketoglutarate (αKG).

renal vascular resistance during salt deprivation (4). However, little is known about the molecular mechanism of the transport of PGE_2 in distal nephron including MD cells.

The OAT family plays important roles in the elimination of a variety of endogenous substances, xenobiotics and their metabolites (9 – 14). We previously reported that human OATs (OAT1 to OAT4) mediate the transport of PGs (8). At present, there is little information on the functional properties of mouse Oat isoforms, particularly mOat3 (19 – 21), although Oat3 knockout mice have been generated several years ago (18). Among the OATs, OAT3 is likely to be a transporter responsible for the basolateral transport of PGE_2 in distal nephron including MD cells based on its broad localization in the rat kidney (15). In this regard, the current results support this possibility. mOat3 mediates both the uptake and the efflux of PGE_2 as shown in Figs. 2 – 4. Furthermore, mOat3 functions as an exchanger for both directions (Figs. 3 and 4). As shown in Fig. 5, mOat3 is localized at the basolateral membrane of proximal tubules, distal tubules including MD cells, and collecting ducts. These characteristics are compatible with the PGE_2 transport pathway in MD cells (Fig. 6).

As shown in Figs. 3 and 4, glutarate, a non-metabolized dicarboxylate, *trans*-stimulated mOat3-mediated PGE_2 transport in both directions. Taking the existence of the outwardly directed dicarboxylate gradient in tubular cells into account, endogenous dicarboxylates such as α-ketoglutarate (αKG) seem to contribute to the uptake of PGE_2 into cells. This supports the idea that Oat3 at the basolateral membrane of distal nephron functions as a re-uptake pathway of released PGE_2. As Pritchard mentioned (39), αKG is the most abundant within the proximal tubular cell. However, to date, there is no information concerning its concentration in distal nephron. Furthermore, energy-utilizing processes are different from segment to segment, based on the observation of ATP production in microdissected nephron segments shown by Uchida and Endou (40). Therefore, we could not exclude the possibility that Oat3 functions as an efflux pathway for PGE_2. As αKG is unlikely to be the endogenous counterion for PGE_2 efflux in MD cells, it seems necessary to identify such an endogenous counterion(s) for PGE_2 efflux in MD cells to further consider the role of PGE_2 as a signal, although the efflux of PGE_2 occurs without the counterion (Fig. 4).

Recently, Soodvilai et al. reported that the exposure of PGE_2 enhanced the OAT3-mediated estrone sulfate transport in isolated rabbit renal proximal tubules (41). Although no PGE_2-receptor isoform was detected in proximal tubules and distal tubules in renal cortex (3), this phenomenon seems compatible for the role of re-uptake of PGE_2 to maintain its extracellular concentration.

The K_m value for PGE_2 (1.48 μM) is different in humans and mice (more than 4-fold difference, ref. 8). The reason for this may be due to the interspecies difference in the interactions of OAT3/Oat3 with this substance or the difference in the expression system, that is, mammalian expression system for hOAT3 (8) versus *Xenopus* oocytes expression system for mOat3 (this study).

The generation of gene knockout animals could provide new information on the contribution of individual transporters in intact organs. Knockout mice for Oat3 have been generated several years ago (18). This model revealed the loss of organic anion transport and indicated the importance of drug uptake of Oat3 in the kidney and choroids plexus (42), although no morphological changes were found. Considering the novel role of mOat3 as a basolateral transport pathway of PGE_2 in MD cells, it would be interesting to observe changes in phenotype in mice under high renin states such as salt deficiency, administration of angiotensin-converting enzyme inhibitors or angiotensin receptor blockers, diuretic administration, or experimental renovascular

hypertension.

Since the molecular cloning of OAT1, first isoform of the OAT family, OATs were recognized mainly as an influx pathway of numerous endogenous and exogenous organic anions (12 – 14). However, recent studies by Aisf et al. unveiled the novel role of OAT3 as an efflux pathway of cortisol in endocrine tissues such as adrenocortical cells (43, 44). Therefore, the maintenance of homeostasis through the efflux of some endogenous substances such as PGs and steroid hormones would be another important role of the OAT family (9).

In conclusion, the current results indicate that mOat3 may play an important role in the basolateral efflux pathway of PGE_2 in the renal tubules including MD cells that may constitute one of the indispensable steps for renin release and the regulation of the TGF mechanism.

Acknowledgments

This work was supported in part by grants from the Ministry of Education, Culture, Sports, Science, and Technology of Japan; the Japan Society for the Promotion of Science; Research on Health Sciences focusing on Drug Innovation from the Japan Health Sciences Foundation; Mutual Aid Corporation for Private Schools of Japan; the Salt Science Research Foundation (No. 0524); the Japan Foundation of Applied Enzymology; Astellas Foundation for Research on Metabolic Disorders; Gout Research Foundation of Japan; The Ichiro Kanehara Foundation; The Shimabara Science Promotion Foundation; Kyorin University School of Medicine (Kyorin Medical Research Award 2006); and Health and Labor Sciences Research Grants for Research on Advanced Medical Technology: Toxicogenomics Project.

References

1 Narumiya S, Sugimoto Y, Ushikubi F. Prostanoid receptors: structures, properties, and functions. Physiol Rev. 1999;79: 1193–1226.
2 Ushikubi F, Sugimoto Y, Ichikawa A, Narumiya S. Roles of prostanoids revealed from studies using mice lacking specific prostanoid receptors. Jpn J Pharmacol. 2000;83:279–285.
3 Breyer MD, Breyer RM. G protein-coupled prostanoid receptors and the kidney. Annu Rev Physiol. 2001;63:579–605.
4 Peti-Peterdi J, Komlosi P, Fuson AL, Guan Y, Schneider A, Qi Z, et al. Luminal NaCl delivery regulates basolateral PGE_2 release from macula densa cells. J Clin Invest. 2003;112:76–82.
5 Schuster VL. Prostaglandin transport. Prostaglandins Other Lipid Mediat. 2002;68-69:633–647.
6 Bao Y, Pucci ML, Chan BS, Lu R, Ito S, Schuster VL. Prostaglandin transporter PGT is expressed in cell types that synthesize and release prostanoids. Am J Physiol Renal Physiol. 2002;282:F1103–F1110.
7 Kimura H, Takeda M, Narikawa S, Enomoto A, Ichida K, Endou H. Human organic anion transporters and human organic cation transporters mediate renal transport of prostaglandins. J Pharmacol Exp Ther. 2002;301:293–298.
8 Nomura T, Chang HY, Lu R, Hankin J, Murphy RC, Schuster VL. Prostaglandin signaling in the renal collecting duct: release, reuptake, and oxidation in the same cell. J Biol Chem. 2005;280:28424–28429.
9 Anzai N, Kanai Y, Endou H. Organic anion transporter family: current knowledge. J Pharmacol Sci. 2006;100:411–426.
10 Sekine T, Miyazaki H, Endou H. Molecular physiology of renal organic anion transporters. Am J Physiol Renal Physiol. 2006;290:F251–F261.
11 Anzai N, Jutabha P, Kanai Y, Endou H. Integrated physiology of proximal tubular organic anion transport. Curr Opin Nephrol Hypertens. 2005;14:472–479.
12 Wright SH, Dantzler WH. Molecular and cellular physiology of renal organic cation and anion transport. Physiol Rev. 2004;84:987–1049.
13 You G. The role of organic ion transporters in drug disposition: an update. Curr Drug Metab. 2004;5:55–62.
14 Burckhardt BC, Burckhardt G. Transport of organic anions across the basolateral membrane of proximal tubule cells. Rev Physiol Biochem Pharmacol. 2003;146:95–158.
15 Kojima R, Sekine T, Kawachi M, Cha SH, Suzuki Y, Endou H. Immunolocalization of multispecific organic anion transporters, OAT1, OAT2, and OAT3, in rat kidney. J Am Soc Nephrol. 2002;13:848–857.
16 Ljubojevic M, Balen D, Breljak D, Kusan M, Anzai N, Bahn A, et al. Renal expression of organic anion transporter OAT2 in rats and mice is regulated by sex hormones. Am J Physiol Renal Physiol. 2007;292:F361–F372.
17 Enomoto A, Takeda M, Shimoda M, Narikawa S, Kobayashi Y, Kobayashi Y, et al. Interaction of human organic anion transporters 2 and 4 with organic anion transport inhibitors. J Pharmacol Exp Ther. 2002;301:797–802.
18 Sweet DH, Miller DS, Pritchard JB, Fujiwara Y, Beier DR, Nigam SK. Impaired organic anion transport in kidney and choroid plexus of organic anion transporter 3 (Oat3 (*Slc22a8*)) knockout mice. J Biol Chem. 2002;277:26934–26943.
19 Ohtsuki S, Kikkawa T, Mori S, Hori S, Takanaga H, Otagiri M, et al. Mouse reduced in osteosclerosis transporter functions as an organic anion transporter 3 and is localized at abluminal membrane of blood-brain barrier. J Pharmacol Exp Ther. 2004;309:1273–1281.
20 Kobayashi Y, Ohshiro N, Tsuchiya A, Kohyama N, Ohbayashi M, Yamamoto T. Renal transport of organic compounds mediated by mouse organic anion transporter 3 (mOat3): further substrate specificity of mOat3. Drug Metab Dispos. 2004;32: 479–483.
21 Bahn A, Ljubojevic M, Lorenz H, Schultz C, Ghebremedhin E, Ugele B, et al. Murine renal organic anion transporters mOAT1 and mOAT3 facilitate the transport of neuroactive tryptophan metabolites. Am J Physiol Cell Physiol. 2005;289:C1075–C1084.
22 Sakata T, Anzai N, Shin HJ, Noshiro R, Hirata T, Yokoyama H, et al. Novel single nucleotide polymorphisms of organic cation transporter 1 (*SLC22A1*) affecting transport functions. Biochem Biophys Res Commun. 2004;313:789–793.
23 Anzai N, Jutabha P, Enomoto A, Yokoyama H, Nonoguchi H,

Hirata T, et al. Functional characterization of rat organic anion transporter 5 (*Slc22a19*) at the apical membrane of renal proximal tubules. J Pharmacol Exp Ther. 2005;315:534–544.
24 Jutabha P, Kanai Y, Hosoyamada M, Chairoungdua A, Kim do K, Iribe Y, et al. Identification of a novel voltage-driven organic anion transporter present at apical membrane of renal proximal tubule. J Biol Chem. 2003;278:27930–27938.
25 Chan BS, Satriano JA, Pucci M, Schuster VL. Mechanism of prostaglandin E2 transport across the plasma membrane of HeLa cells and Xenopus oocytes expressing the prostaglandin transporter "PGT". J Biol Chem. 1998;273:6689–6697.
26 Sweet DH, Chan LM, Walden R, Yang XP, Miller DS, Pritchard JB. Organic anion transporter 3 (*Slc22a8*) is a dicarboxylate exchanger indirectly coupled to the Na^+ gradient. Am J Physiol Renal Physiol. 2003;284:F763–F769.
27 Bakhiya N, Bahn A, Burckhardt G, Wolff NA. Human organic anion transporter 3 (hOAT3) can operate as an exchanger and mediate secretory urate flux. Cell Physiol Biochem. 2003; 13:249–256.
28 Smith WL, Bell TG. Immunohistochemical localization of the prostaglandin-forming cyclooxygenase in renal cortex. Am J Physiol. 1978;235:F451–F457.
29 Harris RC, McKanna JA, Akai Y, Jacobson HR, Dubois RN, Breyer MD. Cyclooxygenase-2 is associated with the macula densa of rat kidney and increases with salt restriction. J Clin Invest. 1994;94:2504–2510.
30 Schnermann J. Cyclooxygenase-2 and macula densa control of renin secretion. Nephrol Dial Transplant. 2001;16:1735–1738.
31 Harris RC, Wang JL, Cheng HF, Zhang MZ, McKanna JA. Prostaglandins in macula densa function. Kidney Int. 1998;67: S49–S52.
32 Schnermann J, Briggs J. Function of the juxtaglomerular apparatus: local control of glomerular hemodynamics. In: Seldin DW, Giebisch G, editors. The kidney. New York: Raven Press; 1985. p. 669–697.
33 Harris RC, Breyer MD. Physiological regulation of cyclooxygenase-2 in the kidney. Am J Physiol Renal Physiol. 2001;281:F1–F11.
34 Yang T, Endo Y, Huang YG, Smart A, Briggs JP, Schnermann J. Renin expression in COX-2-knockout mice on normal or low-salt diets. Am J Physiol Renal Physiol. 2000;279:F819–F825.
35 Castrop H, Schweda F, Schumacher K, Wolf K, Kurtz A. Role of renocortical cyclooxygenase-2 for renal vascular resistance and macula densa control of renin secretion. J Am Soc Nephrol 2001;12:867–874.
36 Traynor TR, Smart A, Briggs JP, Schnermann J. Inhibition of macula densa-stimulated renin secretion by pharmacological blockade of cyclooxygenase-2. Am J Physiol 1999;277:F706–F710.
37 Chaudhari A, Gupta S, Kirschenbaum MA. Biochemical evidence for PGI_2 and PGE_2 receptors in the rabbit renal preglomerular microvasculature. Biochim Biophys Acta. 1990;1053:156–161.
38 Schnermann J, Weber PC. Reversal of indomethacin-induced inhibition of tubuloglomerular feedback by prostaglandin infusion. Prostaglandins. 1982;24:351–361.
39 Pritchard JB. Intracellular alpha-ketoglutarate controls the efficacy of renal organic anion transport. J Pharmacol Exp Ther. 1995;274:1278–1284.
40 Uchida S, Endou H. Substrate specificity to maintain cellular ATP along the mouse nephron. Am J Physiol. 1988;255:F977–F983.
41 Soodvilai S, Chatsudthipong V, Evans KK, Wright SH, Dantzler WH. Acute regulation of OAT3-mediated estrone sulfate transport in isolated rabbit renal proximal tubules. Am J Physiol Renal Physiol. 2004;287:F1021–F1029.
42 Sykes D, Sweet DH, Lowes S, Nigam SK, Pritchard JB, Miller DS. Organic anion transport in choroid plexus from wild-type and organic anion transporter 3 (*Slc22a8*)-null mice. Am J Physiol Renal Physiol. 2004;286:F972–F978.
43 Asif AR, Steffgen J, Metten M, Grunewald RW, Muller GA, Bahn A, et al. Presence of organic anion transporters 3 (OAT3) and 4 (OAT4) in human adrenocortical cells. Pflugers Arch. 2005;450:88–95.
44 Asif AR, Ljubojevic M, Sabolic I, Shnitsar V, Metten M, Anzai N, et al. Regulation of steroid hormone biosynthesis enzymes and organic anion transporters by forskolin and DHEAS treatment in adrenocortical cells. Am J Physiol Endocrinol Metab. 2006; 291:E1351–E1359.

Int. J. Cancer: **119,** 484–492 (2006)

FAST TRACK

L-type amino acid transporter 1 as a potential molecular target in human astrocytic tumors

Hiroshi Nawashiro[1]*, Naoki Otani[1], Nariyoshi Shinomiya[2], Shinji Fukui[1], Hidetoshi Ooigawa[1], Katsuji Shima[1], Hirotaka Matsuo[3], Yoshikatsu Kanai[4] and Hitoshi Endou[4]

[1]*Department of Neurosurgery, National Defense Medical College, Tokorozawa, Saitama, Japan*
[2]*Department of Microbiology, National Defense Medical College, Tokorozawa, Saitama, Japan*
[3]*1st Department of Physiology, National Defense Medical College, Tokorozawa, Saitama, Japan*
[4]*Department of Pharmacology and Toxicology, Kyorin University School of Medicine, Mitaka, Tokyo, Japan*

L-type amino acid transporter 1 (LAT1) is a Na^+-independent neutral amino acid transport agency and essential for the transport of large neutral amino acids. LAT1 has been identified as a light chain of the CD98 heterodimer from C6 glioma cells. LAT1 also corresponds to TA1, an oncofetal antigen that is expressed primarily in fetal tissues and cancer cells. We have investigated for the first time, the expression of the transporter in the human primary astrocytic tumor tissue from 60 patients. LAT1 is unique because it requires an additional single membrane spanning protein, the heavy chain of 4F2 cell surface antigen (4F2hc), for its functional expression. 4F2hc expression was also determined by immunohistochemistry. Kaplan-Meier analyses demonstrated that high LAT1 expression correlated with poor survival for the study group as a whole ($p < 0.0001$) and for those with glioblastoma multiforme in particular ($p = 0.0001$). Cox regression analyses demonstrated that LAT1 expression was one of significant predictors of outcome, independent of all other variables. On the basis of these findings, we also investigated the effect of the specific inhibitor to LAT1, 2-aminobicyclo-2 (2,2,1)-heptane-2-carboxylic acid (BCH), on the survival of C6 glioma cells *in vitro* and *in vivo* using a rat C6 glioma model. BCH inhibited the growth of C6 glioma cells *in vitro* and *in vivo* in a dose-dependent manner. Kaplan-Meier survival data of rats treated with BCH were significant. These findings suggest that LAT1 could be one of the molecular targets in glioma therapy.

Key words: glioma; L-type amino acid transporter (LAT1); BCH

Glioma, especially glioblastoma, is the most common intrinsic brain tumor and with the worst prognosis in human malignancy. The cause of death of glioma patients is not a distant metastasis but the failure of local control of the tumor. The invasive nature of glioma often prevents total surgical excision. Adjuvant therapy for the residual tumor is therefore essential, however, conventional chemotherapy, immunotherapy, and radiotherapy has been proved to be of limited value.[1] Gene therapy for malignant glioma has been expected to be useful; however, no definitive clinical usefulness has been proved. Recently, several candidates for the molecular target of malignant tumors are advocated. One of them is the angiogenic and vascular proliferating factor.[2] The highly proliferating malignant tumor cells may need much substrate such as sugars and amino acids. If a specific upregulation of amino acid transport system in malignant tumor cells do exist, it could be a molecular target for therapy.

L-type amino acid transporter 1 (LAT1) is a Na^+-independent neutral amino acid transport agency and essential for the transport of large neutral amino acids through the plasma membrane.[3,4] LAT1 exhibits high affinity for several nutritionally essential amino acids such as leucine, isoleucine, valine, phenylalanine, tryptophan and methionine. The molecular nature of LAT1 was not characterized until 1998, when using expression cloning, a cDNA encoding a transporter subserving the LAT1 from a C6 rat glioma cell cDNA library was isolated by Kanai *et al.*[3] Since LAT1 is highly regulated in nature and upregulated upon the isolation and cultivation of cells, it is essential to examine the *in vivo* expression of LAT1 in brain tumor tissues.[5,6] The specific antibody to human LAT1, which recognizes both rodent and human LAT1, was generated. Using this antibody, we have investigated for the first time, the expression of the transporter in the human astrocytic tumor tissue. LAT1 is unique because it requires an additional single membrane spanning protein, the heavy chain of 4F2 cell surface antigen (4F2hc), for its functional expression.[3] When coexpressed with 4F2hc, LAT1 transports neutral amino acids with branched or aromatic side chains and does not accept basic amino acids or acidic amino acids.[3] 4F2hc expression was also determined by immunohistochemical staining with a polyclonal rabbit anti-human 4F2hc antibody. All astrocytic tumor cells clearly exhibited positive staining for LAT1 in variable degrees: however, we found strong expression of LAT1 in high-grade astrocytomas. On the basis of these findings, we also investigated the effect of the specific inhibitor to LAT1, 2-aminobicyclo-2(2,2.1)-heptane-2-carboxylic acid (BCH), on the growth of C6 glioma cells *in vitro* and *in vivo* using a rat C6 glioma model.[7]

Material and methods

Patients and tissues

All patients had primary astrocytic tumors of the brain. Patients were treated surgically for the first time between 1990 and 1999 in our hospital. Clinical data were obtained by retrospective chart review. Survival was determined from the date of initial surgery. Follow-up was available for all patients. Informed consent was obtained in all cases. Median follow-up time from resection of initial disease was 40.9 months.

Tumor specimens were obtained by surgical resection in all cases. Formalin-fixed, paraffin-embedded sections were stained with hematoxylin and eosin, and a histological and cytological diagnosis was made.

Histological diagnosis and tumor grading were performed according to the grading system established by WHO.[8] Fifteen specimens were diagnosed as Grade 2, 17 as Grade 3 and 28 as Grade 4 (glioblastoma multiforme (GBM)).

Immunohistochemistry for human LAT1 and 4F2hc in the glioma

LAT1 expression was determined by immunohistochemical staining with an affinity-purified polyclonal rabbit anti-human LAT1 antibody. Oligopeptides corresponding to amino acid residues 497–507 of human LAT1 (CQKLMQVVPQET) and amino acid residues 516–529 of human heavy chain of 4F2 cell surface antigen (4F2hc) (EPHEGLLLRFPYAAC) were synthesized. The N-terminal cystein residues were introduced for conjugation with

***Correspondence to:** Department of Neurosurgery, National Defense Medical College, 3-2 Namiki, Tokorozawa, Saitama 359-8513, Japan. Fax: +81-4-2996-5207. E-mail: nawa1957@ndmc.ac.jp
Received 2 October 2005; Accepted 12 January 2006
DOI 10.1002/ijc.21866
Published online 22 February 2006 in Wiley InterScience (www.interscience.wiley.com).

Publication of the International Union Against Cancer

keyhole limpet hemocyamine. Antipeptide antibodies were produced as described elsewhere.[9] For immunohistochemical analysis, antisera were affinity-purified as described previously.[9]

Immunohistochemical staining was performed on paraffin sections using an avidin–biotinyl peroxidase complex method. Briefly, deparaffinized, rehydrated sections were treated with 0.6% hydrogen peroxide in methanol for 30 min to block endogenous peroxidase activity. After rinsing in 0.05 M tris-buffered saline containing 0.1% tween-20, the sections were incubated with anti-LAT1antiserum (1:250) or anti-4F2hc antiserum (1:500) overnight at 4°C. Thereafter, they were incubated with Envision (+) rabbit peroxidase (DAKO, Carpinteria, CA) for 30 min. The peroxidase reaction was performed using 0.02% 3,3′-diaminobenzidine tetrahydrochloride and 0.01% hydrogen peroxide in 0.05 M tris-HCl buffer, pH 7.4. Finally, nuclear counterstaining was performed with Mayer's hematoxylin. To verify the specificity of immunoreactions by absorption experiments, the tissue sections were treated with primary antibodies in the presence of antigen peptides (200 μg/ml).

Analysis of LAT1 and 4F2hc staining

Immunoreactivity was graded from – to +++ according to the percent of positive cells and the intensity of staining. The percentage of cells expressing LAT1 and 4F2hc was estimated by dividing the number of positively stained astrocytic tumor cells by the total number of tumor cells per high-power field. The cases in which all cells or more than 75% of the cells stained positively were considered diffuse staining: those in which less than 75% of the cells stained were considered patchy staining. More than 1,000 tumor cells were counted to determine the percentage of positive cells. The intensity of staining was determined and recorded as negative, weak, or strong. The cases in which weak patchy or not stained were considered (−); diffuse weak staining were considered (+); strong patchy staining were considered (++); and those strong diffuse staining were considered (+++). According to this grading protocol, 2 observers (HN and NO) of the authors, without prior knowledge of the clinical data, independently graded the staining intensity in all cases. To test the intraobserver variability, all sections were reassessed by one author (HN) after all first measurements had been completed. The time between the first and second assessments was at least 4 weeks. The interobserver variability was determined by comparing the values of the first measurements of 2 authors (HN and NO).

Proliferation rates determined by proliferating cell nuclear antigen immunostaining

The same tumor specimens were analyzed by immnohistochemistry with an anti-proliferating cell nuclear antigen (PCNA) monoclonal antibody (Novocastra Laboratories Ltd., Newcastle upon Tyne, UK). Paraffin-embedded tissue sections (3-μm thick) were employed for immunohistochemistry. After deparaffinization in xylene and blocking of endogenous peroxidase activity with 0.3% hydrogen peroxide in absolute methanol for 30 min at room temperature, the sections were incubated for 1 hr with anti-PCNA monoclonal antibody. The sections were washed with PBS, and treated with biotynyl anti-rabbit immunoglobulin for 10 min, then washed with PBS again and treated with peroxydase-labeled streptavidin for 5 min, and incubated in 3,3′-diaminobenzidine (DAB) solution, and then counterstained with methylgreen. Control study: (*i*) normal brain slices (negative control) (*ii*) adenocarcinoma (positive control) (*iii*) normal rabbit serum was used instead of the specific antibodies. The percentages of PCNA-positive cells were determined by counting 1,000–1,500 cells in at least 2 microphotographs of each section.

Statistical analysis

Survival was analyzed using the Kaplan-Meier method, and prognostic factors were assessed by log-rank analysis. Univariate and multivariate analyses were made of disease-specific survival (based on the number of patients who did not die from glioma). LAT1 and 4F2hc staining score, and other putative prognostic factors (age, gender, tumor histology, PCNA staining index) were used to stratify patients. A stepwise multivariate Cox regression analysis was also performed to further test the independence of LAT1 expression from other parameters. The distribution of the LAT1 score in relation to tumor and patient characteristics was investigated using the χ^2-test. Correlations between variables were obtained using Spearman's rank correlation. All tests were two-sided, and $p < 0.05$ was considered significant.

Cell line and culture condition

C6 rat glioma cell line was purchased from Dainippon Pharmaceutical Company (Osaka, Japan). Cells were maintained in a CO_2 incubator at 37°C by *in vitro* passage at 3–4-day intervals in Ham's F10 medium with 2 mM L-glutamine (GIBCO BRL, Grand Island, NY) supplemented with 15% horse serum (GIBCO BRL) and 2.5% fetal bovine serum (HyClone®). After the cells reached subconfluence, single-cell suspension was obtained by trypsinization and the numbers of cells were counted with a particle counter (Model PC-607, Erma, Tokyo, Japan). Then cell suspensions of desired concentrations were prepared and used for the following experiments.

Evaluation of cell survival in vitro *(colorimetric MTT assay)*

Reagents required for the colorimetric MTT (3-(4,5-dimethylthiazol-2-yl)-2,5-diphenyl tetrasolium bromide) assay were purchased from Chemicon International (Temecula, CA). Cells at a desired concentration were plated in 96-well flat-bottomed tissue culture trays (Falcon) and placed gently until they completely adhered to the bottom. Then the culture medium was replaced by a new one containing a desired concentration of BCH, and its effect on the cell growth was evaluated. The vehicle was culture medium used to introduce the BCH in cell cultures. At the end of the assay, 10 μl of MTT solution was added to each well and cells were incubated at 37°C for 4 hr. Then 100 μl of isopropanol/HCl solution was added to each well to dissolve the MTT formazan. Within an hour, the absorbance at a test wavelength of 595 nm and a reference wavelength of 655 nm ($OD_{595-655}$) was measured on an ELISA plate reader (Bio-Rad, Model 3550 microplate reader).

A rat glioma model

Adult male Wistar rats weighing 200 g were used for this study. Animals were maintained and experiments conducted according to guidelines established by the Institutional Animal Care and Use Committee of National Defense Medical College.

The rats were anesthetized with isoflurane in 30% oxygen and 70% nitrous oxide gas mixture through a facemask. The rats were fixed in a stereotactic head holder in a flat-skull position. A burr hole was made using a 1.4-mm diamond-tipped burr at the following coordinates: 1.5 mm anterior to bregma and 3.0 mm lateral of midline. A needle was inserted into the right caudate nucleus, depth 5.0 mm from the top of skull. C6 cells were prepared fresh from culture to ensure optimal viability of cells during tumor inoculation. Each rat was injected with 1.0×10^6 C6 cells in 10 μl phosphate-buffered saline-glucose medium. After injection, injector remained for 5 min to allow the injected cell suspension to come to equilibrium inside the brain.

For continuous infusion of the tumor inoculation site, each rat was implanted with an osmotic minipump-brain infusion assembly 1 day or 8 days after tumor inoculation. The minipump (average infusion rate, 5.0 l/hr; Alzet model 2ML2; Alza, Palo Alto, CA) was filled with either vehicle alone (saline, control), 50 mM D-mannitol, or a desired concentration (50 mM or 230 mM) of BCH. The brain infusion assembly consisted of a catheter tubing and a stainless steel cannula with two-depth adjustment spacers to obtain stereotaxically correct depth. The tubing-cannula assembly was also filled with the appropriate solution and joined to the pump.

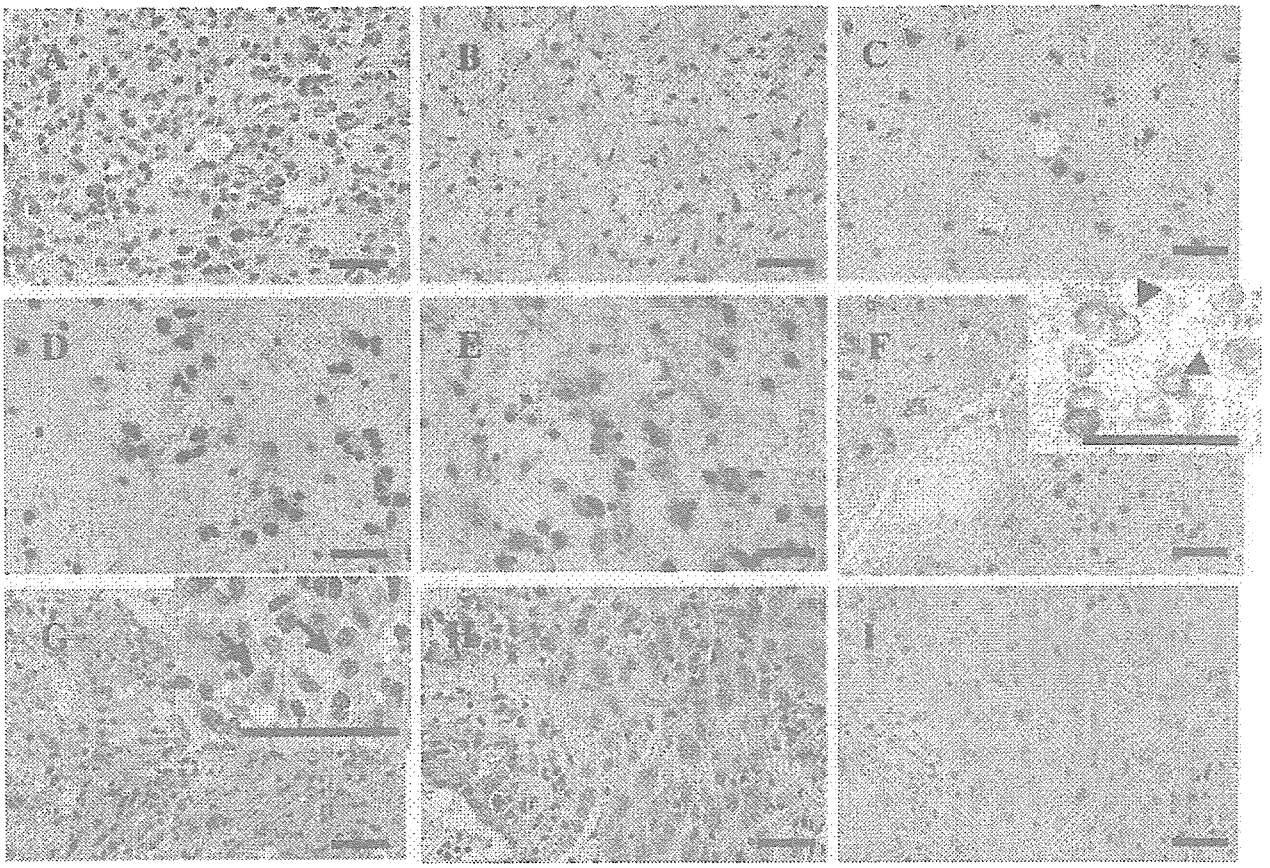

FIGURE 1 – (*a*) Glioblastoma with diffuse weak (+) immunoreactivity for LAT1. (*b*) Low grade glioma with diffuse weak (+) immunoreactivity for LAT1. (*c*) Anaplastic astrocytoma with strong patchy (++) staining for LAT1. (*d*) Anaplastic astrocytoma with strong patchy (++) staining for 4F2hc. (*e*) Anaplastic astrocytoma (the same specimen as shown in *d*) with diffuse strong (+++) staining for LAT1. (*f*) Anaplastic astrocytoma with intense immunoreactivity for LAT1 observed predominantly on the plasma membrane (arrow heads). Inset at higher magnification. (*g*) Glioblastoma with strong diffuse (+++) cytoplasmic staining (arrows) for LAT1. Inset at higher magnification. (*h*) Glioblastoma with strong diffuse (+++) cytoplasmic staining for LAT1. (*i*) In the absorption experiments, the LAT1 immunostainings were diminished, confirming the specificity of the immunoreaction (the same specimen as shown in H). Immunoreactions were visualized with diaminobenzidine and nuclear counterstaining was performed with Mayer's hematoxylin. All bars = 20 μm.

One day or 8 days after tumor inoculation, the cannula was inserted at the inoculation site and secured in position with dental cement. The osmotic pump was housed in a subcutaneous pocket in the midscapular area of the back of the rat for 28 days. Animals recovered from anesthesia and resumed their previous activity in cages. The animals were housed individually to prevent dislodging of the brain infusion assembly.

Fifty-one rats were divided into 6 experimental groups. Group 1 (n = 9) were given 230 mM of BCH 1 day after tumor inoculation. Group 2 (n = 9) were given the saline 1 day after tumor inoculation. In Group 3 (n = 7), animals were given 230 mM of BCH 8 days after tumor inoculation. Group 4 (n = 12) received 50 mM of BCH 8 days after tumor inoculation. This dose was selected because cell survival was disturbed *in vitro* when BCH was added at a concentration of more than 25 mM. Group 5 (n = 7) were given the saline 8 days after tumor inoculation. Group 6 (n = 7) were given 50 mM D-mannitol 8 days after tumor inoculation.

After tumor inoculation, the body weight of rats was measured and recorded every day. All survivors were sacrificed 22 days after implantation. They were deeply anesthetized with intraperitoneal pentobarbital (100 mg/kg). Animals were perfused transcardially with normal saline followed by 4% buffered paraformaldehyde. The brains were removed and embedded in paraffin after fixation in 4% buffered paraformaldehyde followed by 0.1 mmol/l PBS (pH 7.4) for 24 hr at 4°C. Serial coronal sections (5-μm-thick) were prepared. The serial sections were mounted onto silanated slides and were used for histology and histochemistry. The sections were stained with hematoxylin and eosin to confirm the tumor. The same tumor specimens were analyzed by immunohistochemistry with an anti-PCNA monoclonal antibody as described above. The extent of the tumor at 20 predetermined levels was measured with the computer-assisted image analyzing system (NIH image 1.57). The tumor volume was calculated by taking the sum of the tumor areas of the different brain slices times the thickness of the slices. Tumor volumes and the percentages of PCNA-positive cells in each animals were analyzed by analysis of variance (ANOVA) followed by the Bonferroni/Dunn test to ascertain significance between groups. The body weight of each animal was analyzed by repeated-measures ANOVA. Statistical significance was set at $p < 0.05$.

Results

Sixty specimens were obtained from 60 patients with primary astrocytic gliomas. Twenty-nine patients were male and 31 were female. They ranged from 11 to 88 yr in age (mean, 45.1 years ± 19.3). All patients had Karnofsky performance scores of at least 70 at diagnosis. Patients were treated with surgery and adjuvant chemoradiation therapy (consisting of ACNU, interferon β, local

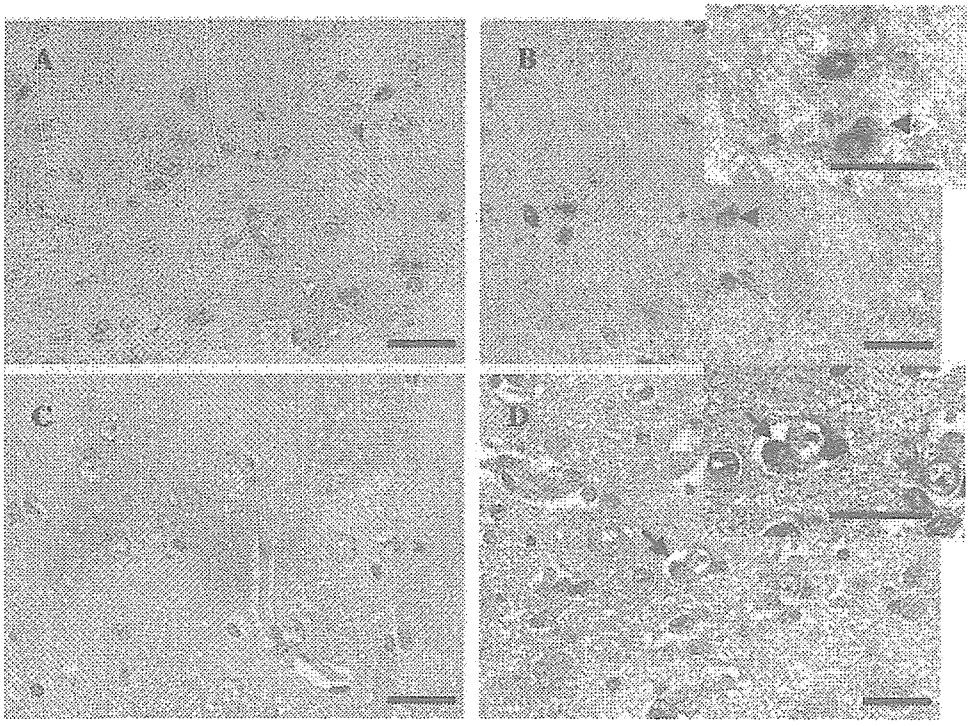

FIGURE 2 – (*a*) Control LAT1 staining on normal uninvolved brain. (*b*) Glioblastoma cells of the same patient in the border zone with strong staining for LAT1 showing perineuronal satellitosis (arrow heads). (*c*) Control 4F2hc staining on normal uninvolved brain in the same patient. (*d*) Glioblastoma cells of the same patient in the border zone with weak staining for 4F2hc showing perineuronal satellitosis (arrows). All bars = 20 μm.

TABLE I – CORRELATION OF LAT1 AND 4F2hc STAINING WITH CLINICAL AND HISTOPATHOLOGICAL FEATURES OF ASTROCYTIC TUMORS

	LAT1			*p*	4F2hc			*p*
	(+) (*n* = 21)	(++) (*n* = 18)	(+++) (*n* = 21)		(+) (*n* = 27)	(++) (*n* = 22)	(+++) (*n* = 11)	
Age (yr)								
0–19	6	2	0	0.0658	4	4	0	0.731
20–39	5	4	3		6	4	2	
40–59	7	8	8		11	8	4	
60+	3	4	10		6	6	5	
Tumor histology								
Low-grade astrocytoma	10	4	1	0.0059	8	7	0	0.1074
AA	4	8	5		10	4	3	
GBM	7	6	15		9	11	8	
Gender								
Male	9	6	14	0.0953	15	7	7	0.1354
Female	12	12	7		12	15	4	
PCNA index (%)								
<5	7	4	0	0.0075	6	5	0	0.0264
5–30	10	10	8		16	9	3	
>30	4	4	13		5	8	8	
4F2hc								
(+)	12	9	6	0.0098				
(++)	8	8	6					
(+++)	1	1	9					

external beam radiation) for all patients with GBM or anaplastic astrocytoma and adjuvant radiation therapy for most patients with low-grade astrocytoma. There were 28 GBMs, 17 anaplastic astrocytomas and 15 low-grade fibrillary astrocytomas.

Qualitative immunohistochemical analysis for LAT1 and 4F2hc

LAT1 and 4F2hc immunoreactivity was observed in all the tumor specimens examined. LAT1 immunostaining was observed predominantly on the plasma membrane and astrocytic process (Figs. 1*c* and 1*f*). In cases of strong diffuse LAT1 staining in tumor cells, intense cytoplasmic staining was also evident (Figs. 1*g* and 1*h*). In sections containing areas of normal cortex adjacent to the tumor, infiltrating tumor cells showed more intense LAT1 staining (Fig. 2*b*). Examples of LAT1 and 4F2hc immunostaining of the same specimen are shown in Figures 1*d* and 1*e*. In the absorption experiments in which tissue sections were treated with primary antibodies in the presence of antigen peptides, the immunostaining was drastically decreased, confirming the specificity of the immunoreaction (Fig. 1*i*). The nuclear staining for LAT1 might be artifactual; however, the nuclear and perinuclear staining

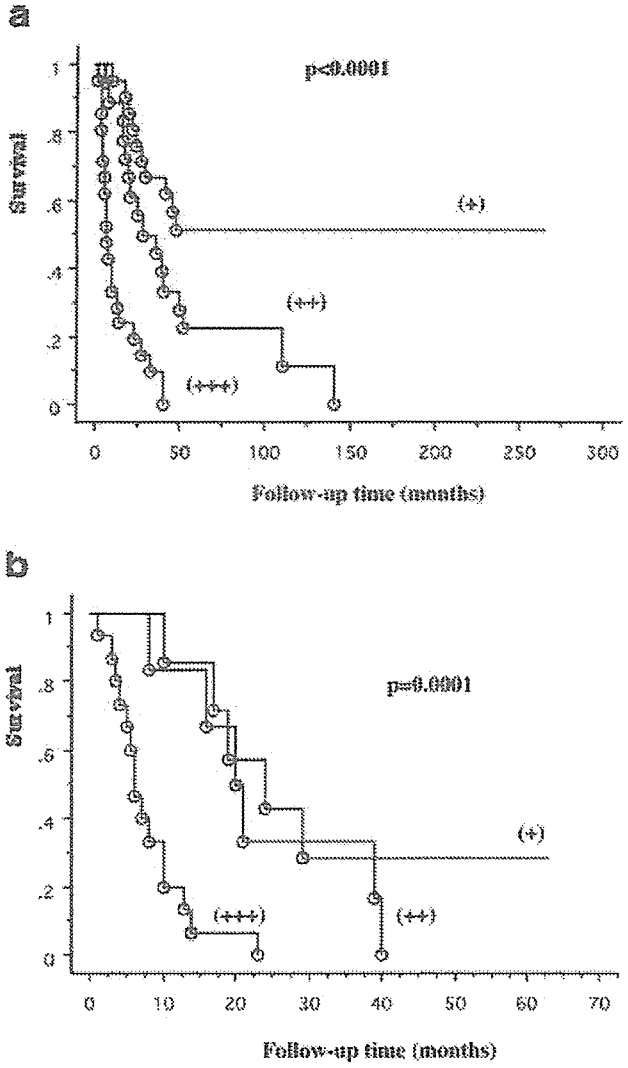

FIGURE 3 – (*a*) Actuarial survival (Kaplan-Meier method) of patients with astrocytoma whose tumors had LAT1 immunostaining of (+), (++) or (+++). (*b*) Actuarial survival (Kaplan-Meier method) of patients with GBM whose tumors had LAT1 immunostaining of (+), (++) or (+++).

was also decreased in the absorption experiments. LAT1 and 4F2hc immunostaining on normal uninvolved brain are shown in Figures 2*a* and 2*c*. No significant immunostaining in neurons or astrocytes was seen in the uninvolved normal brain. The intraobserver reproducibility of scoring was high (correlation coefficient, 0.93; $p < 0.0001$; coefficient of variance, 29.7%). The interobserver reproducibility of scoring was also high (correlation coefficient, 0.9; $p < 0.001$; coefficient of variance, 31.1%).

Correlation of LAT1 and 4F2hc staining with clinical and histopathological features

LAT1 immunostaining did not correlate with patient age or gender (Table I). However, the intensity of LAT1 staining was greater in GBMs than in low-grade astrocytomas (Table I). The grade of LAT1 staining increased with glioma grade, and this finding was statistically significant. The grade of LAT1 staining correlated statistically with PCNA index ($p = 0.0075$) and with 4F2hc staining ($p = 0.0098$) (Table I). The grade of 4F2hc staining also correlated statistically with PCNA index ($p = 0.0264$).

TABLE II – UNIVARIATE ANALYSIS OF PROGNOSTIC FACTORS FOR SURVIVAL

	No. of patients	3-yr survival (%)	*p* (log rank)
Age (yr)			
0–19	8	75.0	0.0006
20–39	12	41.7	
40–59	23	43.5	
60+	17	5.9	
Tumor histology			
Low-grade astrocytoma	15	80.0	<0.0001
AA	17	35.3	
GBM	28	10.7	
Gender			
Male	29	20.7	0.0227
Female	31	54.8	
PCNA index (%)			
<5	11	63.6	0.0392
5–30	28	39.3	
>30	21	19.0	
LAT1			
(+)	21	61.9	<0.0001
(++)	18	44.4	
(+++)	21	0.0	
4F2hc			
(+)	27	40.7	0.0183
(++)	22	45.5	
(+++)	11	9.1	

Correlation with patient survival

Kaplan-Meier survival plots for all patients showed a statistically significant association between high grade of LAT1 staining and poor outcome ($p < 0.0001$; Fig. 3*a*, Table II). Because survival of patients with glioma has been associated with several clinicopathological variables, we attempted to define the relative contribution of LAT1 immunostaining to survival by using multivariate Cox regression analyses with 6 variables (age, tumor histology, gender, PCNA index, LAT1 staining and 4F2hc staining). In the initial univariate analysis, age ($p = 0.0006$), tumor histology ($p < 0.0001$), 4F2hc staining ($p = 0.0183$), gender ($p = 0.0227$), PCNA index ($p = 0.0392$), and LAT1 staining ($p < 0.0001$) were all significant (Table II). For the multivariate analysis, we used the backward stepwise (Wald) method, in which variables were removed at each step, based on a 0.05 level of significance. At the final step, the last 3 variables, tumor histology ($p < 0.0001$), LAT1 staining ($p = 0.0004$), and age of patients ($p = 0.0244$) were found to be significant and independent of one another (Table III).

To evaluate the effect of high LAT1 staining grade within tumor grades, we analyzed the GBM subgroup for an association between LAT1 staining and survival. We found that GBM patients with tumors of high LAT1 staining grade had a statistically significant poorer prognosis than did those with tumors of low LAT1 staining grade ($p = 0.0001$ log-rank) (Fig. 3*b*). We also found that patients with low grade atrocytomas of high LAT1 staining had a statistically poor prognosis ($p = 0.0035$ log-rank). In the anaplastic astrocytoma group, no difference in survival was found, but the numbers of patients in this group was too small for accurate statistical sampling.

In vitro *effect of BCH on the survival of C6 glioma cells*

First, to ascertain the linearity of the MTT assay in C6 glioma cells, we performed serial dilution of the cells, and effect of cell number on the colorimeter reading was observed. The $OD_{595-655}$ well correlated with the actual number of the viable cells in the tested range. Accordingly, the cell number to give $OD_{595-655}$ value of 0.5 (namely 25,000 cells/well) was used for the following experiment.

Effect of the various concentration of BCH (from 1 to 100 mM) on the survival of C6 glioma cells was serially observed by MTT assay (Fig. 4). In the control (without BCH), cells continuously